(12) FC

SYSTEMS, SCIENCE AND SOFTWARE

SSS-R-76-2727

PREDICTION AND MATCHING OF TELESEISMIC GROUND MOTION (BODY AND SURFACE WAVES) FROM THE NTS MAST EXPLOSION

T. G. Barker
T. C. Bache
J. T. Cherry
N. Rimer
J. M. Savino

Topical Report

Sponsored by

Advanced Research Projects Agency
ARPA Order No. 2551

This research was supported by the Advanced Research Projects Agency of the Department of Defense and was monitored by AFTAC/VSC, Patrick AFB FL 32925, under Contract No. F08606-75-C-0045.

February 6, 1976

P. O. BOX 1620, LA JOLLA, CALIFORNIA 92038, TELEPHONE (714) 453-0060

SYSTEMS, SCIENCE AND SOFTWARE

SSS-R-76-2727

PREDICTION AND MATCHING OF TELESEISMIC GROUND MOTION (BODY AND SURFACE WAVES) FROM THE NTS MAST EXPLOSION

T. G. Barker
T. C. Bache
J. T. Cherry
N. Rimer
J. M. Savino

Topical Report

Sponsored by

Advanced Research Projects Agency
ARPA Order No. 2551

This research was supported by the Advanced Research Projects Agency of the Department of Defense and was monitored by AFTAC/VSC, Patrick AFB FL 32925, under Contract No. F08606-75-C-0045.

February 6, 1976

P. O. BOX 1620, LA JOLLA, CALIFORNIA 92038, TELEPHONE (714) 453-0060

UNCLASSIFIED

SECURITY CLASSIFICATION OF THIS PAGE (When Data Entered)

REPORT DOCUMENTATION PAGE

READ INSTRUCTIONS BEFORE COMPLETING FORM

1. REPORT NUMBER

2. GOVT ACCESSION NO.

3. RECIPIENT'S CATALOG NUMBER

4. TITLE (and Subtitle)

PREDICTION AND MATCHING OF TELESEISMIC GROUND MOTION (BODY AND SURFACE WAVES) FROM THE NTS MAST EXPLOSION.

5. TYPE OF REPORT & PERIOD COVERED

Topical Report

6. PERFORMING ORG. REPORT NUMBER

SSS-R-76-2727

7. AUTHOR(s)

T. G. Barker, T. C. Bache, J. T. Cherry, N. Rimer and M. Savino

8. CONTRACT OR GRANT NUMBER(s)

F08606-75-C-0045

9. PERFORMING ORGANIZATION NAME AND ADDRESS

Systems, Science and Software
P. O. Box 1620
La Jolla, California 92038

10. PROGRAM ELEMENT, PROJECT, TASK AREA & WORK UNIT NUMBERS

Program Code No. 6F10
ARPA Order [illegible]-2551

11. CONTROLLING OFFICE NAME AND ADDRESS

VELA Seismological Center
312 Montgomery Street
Alexandria, Virginia 22314

12. REPORT DATE

Feb[illegible]1976

13. NUMBER OF PAGES

60

14. MONITORING AGENCY NAME & ADDRESS (if different from Controlling Office)

15. SECURITY CLASS. (of this report)

Unclassified

15a. DECLASSIFICATION/DOWNGRADING SCHEDULE

16. DISTRIBUTION STATEMENT (of this Report)

Approved for public release; distribution unlimited.

17. DISTRIBUTION STATEMENT (of the abstract entered in Block 20, if different from Report)

18. SUPPLEMENTARY NOTES

19. KEY WORDS (Continue on reverse side if necessary and identify by block number)

Explosion Seismology
MAST Explosion
Explosion Source Modeling
Body and Surface Waves
Earth Structure

20. ABSTRACT (Continue on reverse side if necessary and identify by block number)

This report presents the results of a theoretical prediction of the teleseismic body and surface wave signatures of the NTS underground explosion, MAST, and a detailed comparison of the predicted waveforms with seismograms recorded at stations of the Special Data Collection System (SDCS). This study involves a comprehensive analysis of the MAST explosion, including computer modeling of the close-in nonlinear ground motion produced by this event, propagation of the resultant stress waves through the appropriate → next page

DD FORM 1 JAN 73 1473 EDITION OF 1 NOV 65 IS OBSOLETE

UNCLASSIFIED

SECURITY CLASSIFICATION OF THIS PAGE (When Data Entered)

cont.

earth structures and computation of seismograms recorded at designated teleseismic stations.

Comparison of theoretical and observed short- and long-period seismograms were made with respect to amplitude, waveform and travel time. Travel times were closely matched as were the waveforms for surface waves. For body waves a number of the SDCS stations are within the triplication range and the waveform match is far from ideal. Still, amplitudes for both body and surface waves were matched to within 50 percent and were much closer in most cases.

TABLE OF CONTENTS

LIST OF FIGURES

I. INTRODUCTION

This report presents the results of a theoretical prediction of the teleseismic body and surface wave signatures of the recent underground explosion, MAST, and a detailed comparison of the predicted waveforms with seismograms recorded at stations of the Special Data Collection System (SDCS). This study represents a comprehensive analysis of the MAST event involving computer modeling of the close-in nonlinear ground motion produced by the explosion, propagation of the resultant stress waves through the appropriate earth structures and computation of seismograms recorded at designated teleseismic stations.

One of the many important questions that this experiment addresses is, "What pre-shot measurements of the near source medium are required in order to be able to predict the seismically determined yield of a nuclear device to within some specified range?"

Fundamental to the prediction is the calculation of the explosion reduced displacement potential (RDP) which represents the source coupling into elastic waves. A brief description of the constitutive model, material properties and the RDP is given in Section II.

The teleseismic ground motion predictions and comparison to observations are discussed in Section III. For all predictions the source calculation was held fixed and attention was directed to selecting earth models appropriate to the source-receiver travel paths. The predictions were done in two stages; an initial prediction in which standard earth models were used and a revised prediction for which the data were carefully examined and refined earth models were constructed. These refined models should allow quite accurate preshot predictions of future NTS events. In fact,

the procedures followed are applicable to any source-receiver pair.

Comparison of theoretical and observed short and long period seismograms were made with respect to amplitude, waveform and travel time. Travel times were closely matched as were the waveforms for surface waves. For body waves a number of the SDCS stations are within the triplication range and the waveform match is far from ideal. Still, amplitudes for both body and surface waves were matched to within 50 percent and were much closer in most cases. A brief summary of the results and the major lessons learned from this exercise is given in Section IV.

II. CALCULATION OF THE EQUIVALENT ELASTIC SOURCE

Coupling of the nuclear explosion, MAST, into elastic waves was computed using the one-dimensional finite difference code, SKIPPER. MAST was detonated in rhyolite at Pahute Mesa. The reduced displacement potential (RDP) or equivalent elastic source representation of the explosion is dependent on the material properties and constitutive behavior used in the calculation. These, together with the RDP, are described in this section.

Many material properties were able to be taken from the MAST Containment Evaluation Panel (CEP) data synopsis of June 18, 1975. These include bulk density, grain density, water content, degree of saturation, P wave velocity, depth of burial and effective overburden density. Additional material properties data are required, however, in order to obtain the RDP. In particular, no information was available from the CEP document on shear modulus, bulk modulus, or material strength.

The P wave velocity given by the CEP document for the near source rock environment was 4.2 km/sec. Data was also available for HALFBEAK, a shot detonated previously in a similar rhyolite medium, which showed a Poisson's ratio of approximately 0.18. The density of the MAST rhyolite at shot point, from the CEP document, was 2.45 gm/cc. This information is sufficient to derive the bulk and shear moduli, k and μ, of the material:

$$k = \rho \frac{\alpha^2}{3} \left[\frac{1+\sigma}{1-\sigma}\right] = 207 \text{ kbar} ,$$

$$\mu = \rho \frac{\alpha^2}{2} \left[\frac{1-2\sigma}{1-\sigma}\right] = 169 \text{ kbar} .$$

The choice of material strength was the last and most serious issue to be resolved. The material strength, Y, was

assumed to be related to the stress state $\bar{P}$ according to

$$Y = \left[Y_0 + Y_m \frac{\bar{P}}{\bar{P}_m}\left(2 - \frac{\bar{P}}{\bar{P}_m}\right)\right]\left(1 - \frac{e}{e_m}\right), \quad \bar{P} < \bar{P}_m,\ e < e_m ,$$

$$Y = \left(Y_0 + Y_m\right)\left(1 - \frac{e}{e_m}\right), \quad \bar{P} > \bar{P}_m,\ e < e_m ,$$

$$Y = 0 , \quad e > e_m ,$$

where Y_0, Y_m, $\bar{P}_m$ and e_m are material parameters.

Since rhyolite is a relatively strong, competent rock we decided, in the absence of any rhyolite strength measurements, to use the strength data obtained from tests on Hardhat granite (Heard, 1970). A reasonable fit to Heard's granite data is obtained by

$$Y_0 = 0.3 \text{ kbar},$$

$$\bar{P}_m = 9.0 \text{ kbar},$$

$$Y_m = 7.7 \text{ kbar}.$$

The value for the melt energy was chosen to be 2×10^{10} ergs/gm.

The calculation of the RDP was then performed using the technique presented by Cherry, et al. (1975a). Figure 2.1 shows the amplitude spectrum of the reduced velocity potential $|\hat{\Psi}(\omega)|$. This equivalent elastic source, scaled to the yield appropriate for MAST, will be used for all the synthetic seismogram calculations which are presented in the following sections.

We should emphasize that two fundamental material properties representative of the MAST near source rock environment were not available from the CEP document. These were

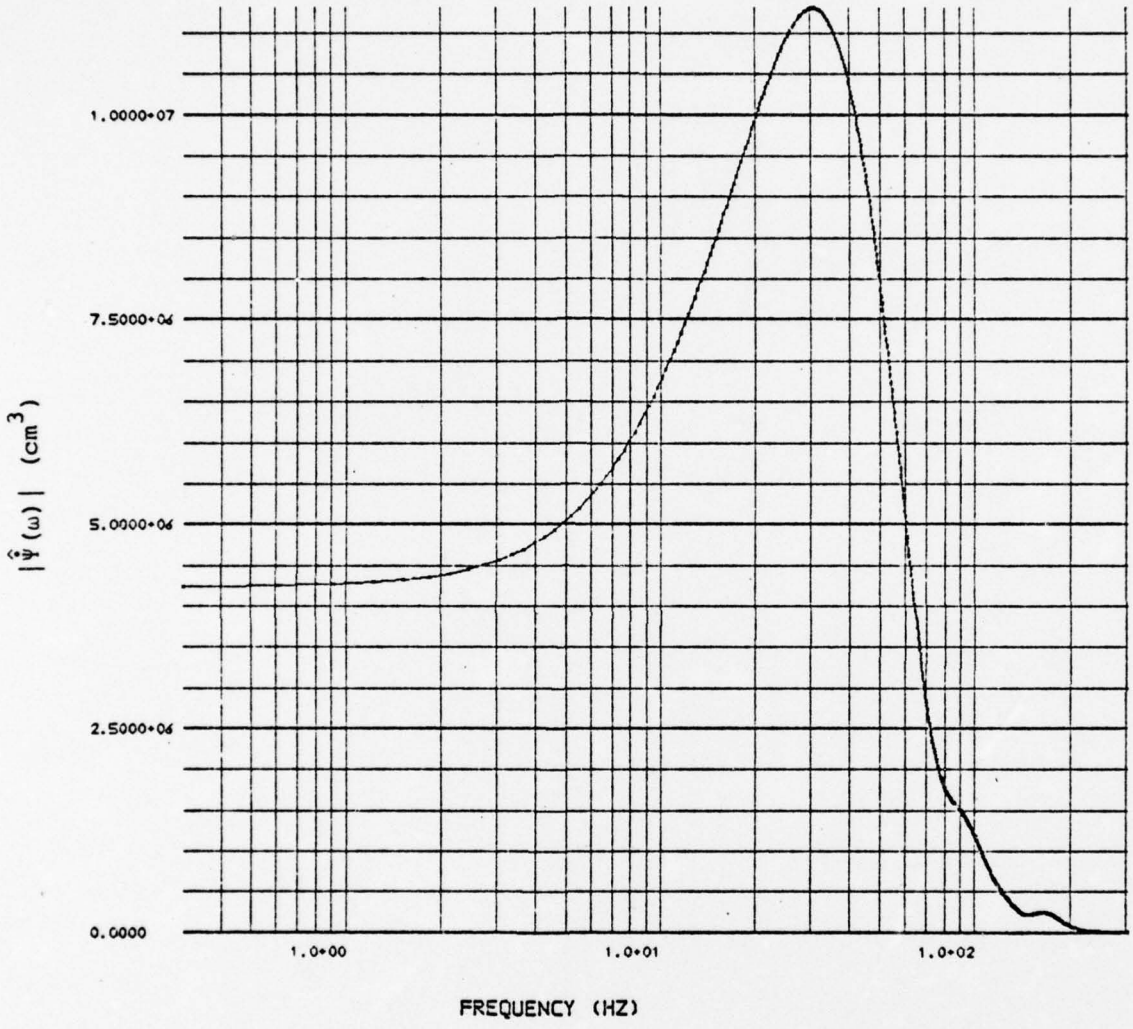

Figure 2.1. The spectral amplitude of the equivalent elastic source for MAST, scaled to 0.02 kt.

Poisson's ratio and material strength. Poisson's ratio was estimated from measurements on the rhyolite from HALFBEAK. Material strength was obtained from strength measurements on Hardhat granite. We did not arbitrarily guess at the material properties which were not available from the CEP document. We chose those properties from what we felt were measurements on representative rock types.

III. TELESEISMIC GROUND MOTION PREDICTIONS FOR THE MAST EVENT

It was requested that S^3 predict the short and long period seismograms recorded for the MAST event at five specified SDCS stations. An initial prediction was made using the best available information for the rock properties at the working point and the near source geology. Standard earth models were used for the propagation path. Upon comparing our predictions to the actual data, we concluded that much, if not most, of the observed discrepancy was due to propagation path effects. Improved modeling of the propagation path is also expected to lead to improved predictions of future events.

In this section we summarize our initial predictions of MAST and the comparison with data. After studying the comparison we made adjustments to our models of the propagation path and the improved results are also summarized.

3.1 COMPUTATIONAL METHODS

The computational method for the prediction of body waves employs the following:

1. The reduced displacement potential (RDP) is computed by our spherically symmetric, one-dimensional finite difference code (SKIPPER).

2. The RDP is input to a code which computes the detailed crustal reverberations for an equivalent elastic source buried in a stack of plane elastic layers (see Appendix B, Bache, et al., 1975b for the theory).

3. Detailed crustal reverberations at the receiver are computed using the method of Haskell (1962).

4. Travel through the upper mantle is computed by generalized ray theory as implemented by Helmberger and described in Wiggins and Helmberger (1974).

5. The desired sensing instrument transfer function is applied to the ground motion.

For surface waves, steps 2-4 are replaced by:

2. The Rayleigh wave dispersion data and amplitude excitation for a plane layered earth model is computed using the method of Harkrider (1964, 1970).

3. The source time history is convolved with the earth response function.

3.2 DATA AND MODELS

The pertinent data were obtained from the following sources:

1. The material properties of the source region were primarily from the MAST CEP data synopsis as described in Section II.

2. The velocity-depth profile for the region above the working point was mainly deduced from the MAST CEP report. In addition, we obtained a log to a depth of 2.3 km of the nearby hole UE19d from Dick Ramspot of LLL. This was used to construct a profile to that depth. The remainder of the crustal model for the body wave calculations is based on an average basin and range crust of Hill and Pakiser (1967). Table 3.1 tabulates the source crustal structure.

3. Since we had little or no information about crustal structure at each of the receiver locations specified by the Project Officer, the same average crustal model was used at all stations for the body wave calculations (see Table 3.2).

4. For the initial prediction of body waves, two upper mantle models were used. These are HWNE from Helmberger and Wiggins (1971) and an unpublished model by Anderson, Hart and Jordan called C2AJ. Detailed studies of data recorded at stations on a northerly azimuth and in the distance range 30-36° from NTS found C2AJ, slightly modified, to be the preferred model. At the time of the first prediction we had not accumulated enough experience at other azimuths and distances to make a reliable selection of an appropriate model.

TABLE 3.1

SOURCE REGION CRUSTAL STRUCTURE

Depth (km)	Thickness (km)	V_p (km/sec)	V_s (km/sec)	ρ (gm/cm^3)
0.076	0.076	2.96	1.7	2.0
0.128	0.052	1.84	1.0	1.5
0.173	0.045	2.03	1.1	1.6
0.555	0.382	4.57	2.6	2.5
0.649	0.094	2.75	1.5	1.9
0.783	0.134	3.75	2.1	2.3
1.133	0.350	4.26	2.4	2.38
1.584	0.451	4.80	2.7	2.65
1.728	0.144	4.30	2.4	2.55
1.778	0.050	3.85	2.1	2.50
2.100	0.322	4.40	2.4	2.58
6.000	3.9	4.7	2.7	2.60
12.000	6.0	5.4	2.8	2.70
20.000	8.0	6.0	3.5	2.8

TABLE 3.2

RECEIVER REGION CRUSTAL STRUCTURE

Depth (km)	Thickness (km)	V_p (km/sec)	V_s (km/sec)	ρ (gm/cm^3)
2.58	2.58	3.67	2.31	2.40
4.84	2.26	5.42	3.27	2.60
11.61	6.77	5.80	3.45	2.60
20.00	8.39	6.00	3.50	2.80

5. For the revised predictions of body waves, all features of the calculation were held the same except different earth upper mantle models were used. The new models were a modified version of HWNE and a modified version of HWA (Wiggins and Helmberger (1973)). The modifications were primarily motivated by a study of the MAST waveforms recorded at the SDCS sites.

6. For the initial predictions of surface waves the earth model CIT109 (Archambeau, Flinn and Lambert (1969)) was used, mainly because it was computationally convenient. However, this model was primarily based on inversion of body wave data and the crustal layers were meant to be generally applicable to shield areas.

7. For the revised Rayleigh wave predictions the procedure was quite direct. Theoretical models generally appropriate to the SDCS sites of interest were selected (CIT109 from Archambeau, et al., 1969 for the shield station WH2YK; a model by McEvilly, 1964, for the others). These models were then perturbed to make the theoretical dispersion closely match the observed dispersion at each station. This station specific theoretical model was then used for the predictions together with an anelastic attenuation model proposed by Tryggvason (1965).

8. The instrument transfer functions were those provided by the Project Officer.

3.3 SITE CORRECTIONS FOR BODY WAVES

Incidental to the predictions, we have been evaluating the quality (for short period observations) of the SDCS stations at which the predictions are being made. The station quality is quantized in terms of (1) the amount of energy converted to tangential ground motion; (2) the coda length which is representative of internal reflection and scattering at the receiver, and (3) the amplitude coupling of the station. The latter is a quantization of that portion of the amplitude response of a station which is independent of azimuth and distance. See Appendix A for details.

The first conclusion from our station quality estimate is that the FNWV site is of low quality and its usefulness (for short period observations) to the SDCS network should be reevaluated. We need to obtain more data to firmly evaluate the other stations but are in the process of doing so.

3.4 COMPARISON BETWEEN THEORETICAL AND OBSERVED P WAVES

The comparison between our theoretical and the observed seismograms will now be presented. In Figs. 3.1 and 3.2 the initial short period predictions are shown together with the observations. Computed seismograms for the two upper mantle models C2AJ and HWNE are shown. From both the theoretical and observed records two amplitudes were measured. The first is the "b" amplitude which is the peak-to-peak amplitude of the first cycle on the record, corrected for the instrument response at the apparent period (i.e., twice the time separation between the measured peaks). The second is denoted the "d" phase. The nomenclature arises from the convention for measuring m_b followed for the LRSM network wherein the maximum cycle in the first few cycles on the wave train is measured. The cycle used for this amplitude is indicated on each seismogram.

The comparison between theoretical and observed "b" and "d" phases from Figs. 3.1 and 3.2 are shown in Figs. 3.3 and 3.4. Examining the wave form comparison in Figs. 3.1 and 3.2 we conclude that many of the important features of the seismograms are predicted by the model but that the comparison is far from ideal. The theoretical b amplitudes are substantially smaller than the observed. Our models should be most accurate in predicting this portion of the wave train. The agreement between d amplitudes, the phase from which conventional m_b is determined, is somewhat better. However, this is to some extent fortuitous since all the interfering phases which contribute to the d amplitude do not appear to be properly included in our calculations.

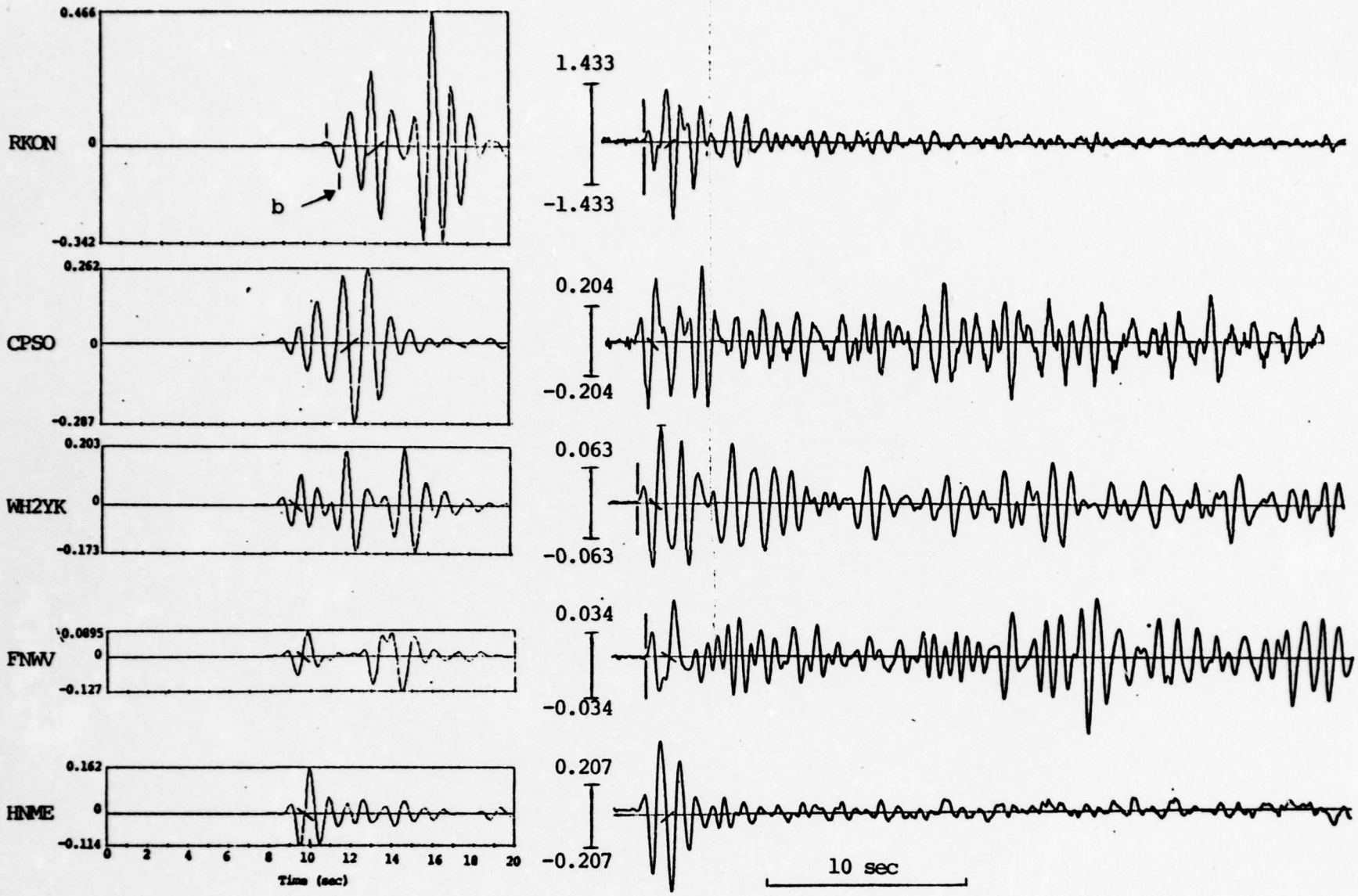

Figure 3.1. Comparison of theoretical (left) and observed (right) seismograms for MAST at five SDCS stations. The upper mantle model for the theoretical calculations is C2AJ. The amplitude scale is indicated in microns at 1 Hz.

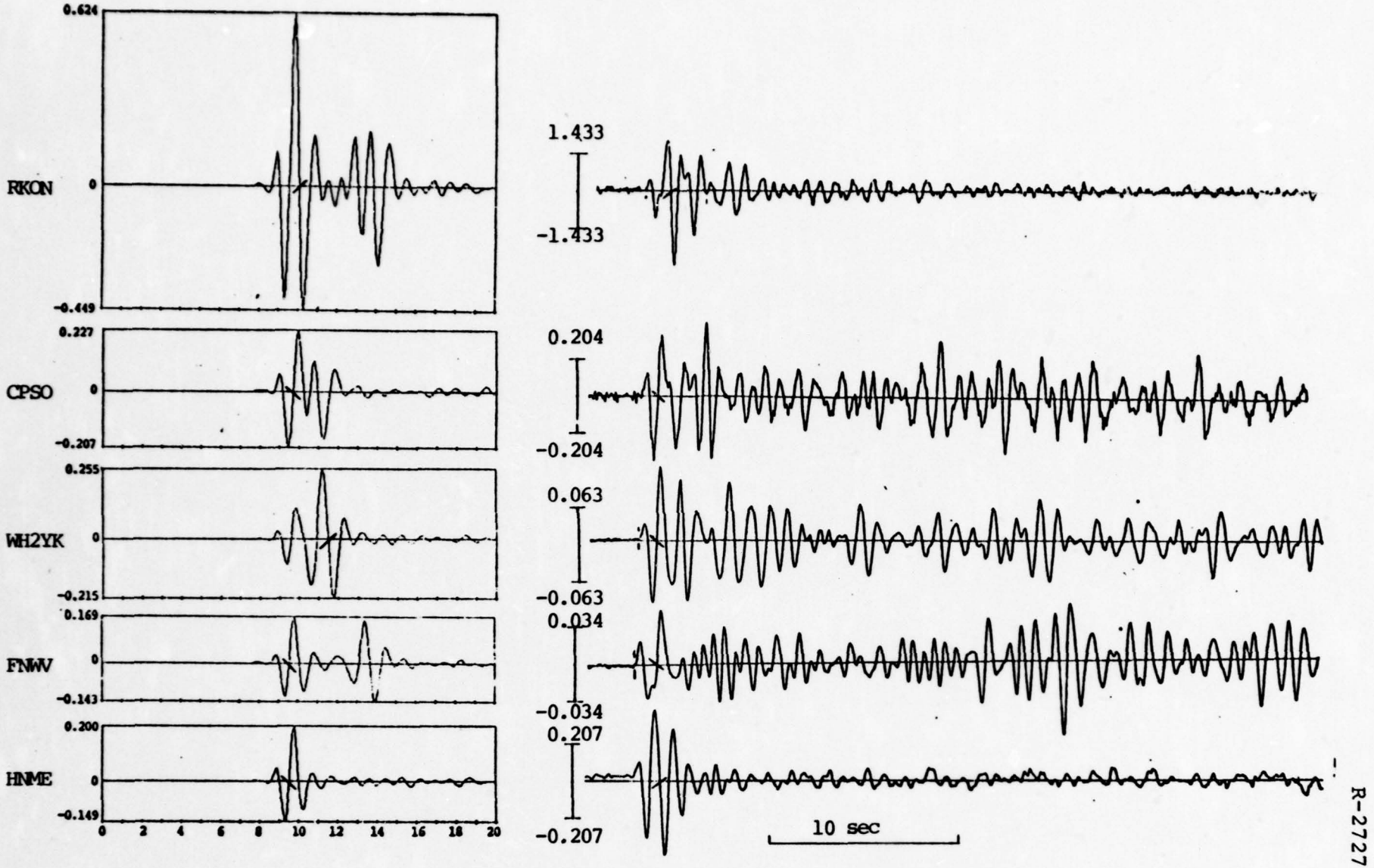

Figure 3.2. Comparison of theoretical (left) and observed (right) seismograms for MAST at five SDCS stations. The upper mantle model used for the theoretical calculations is HWNE. The amplitude scale is indicated in microns at 1 Hz.

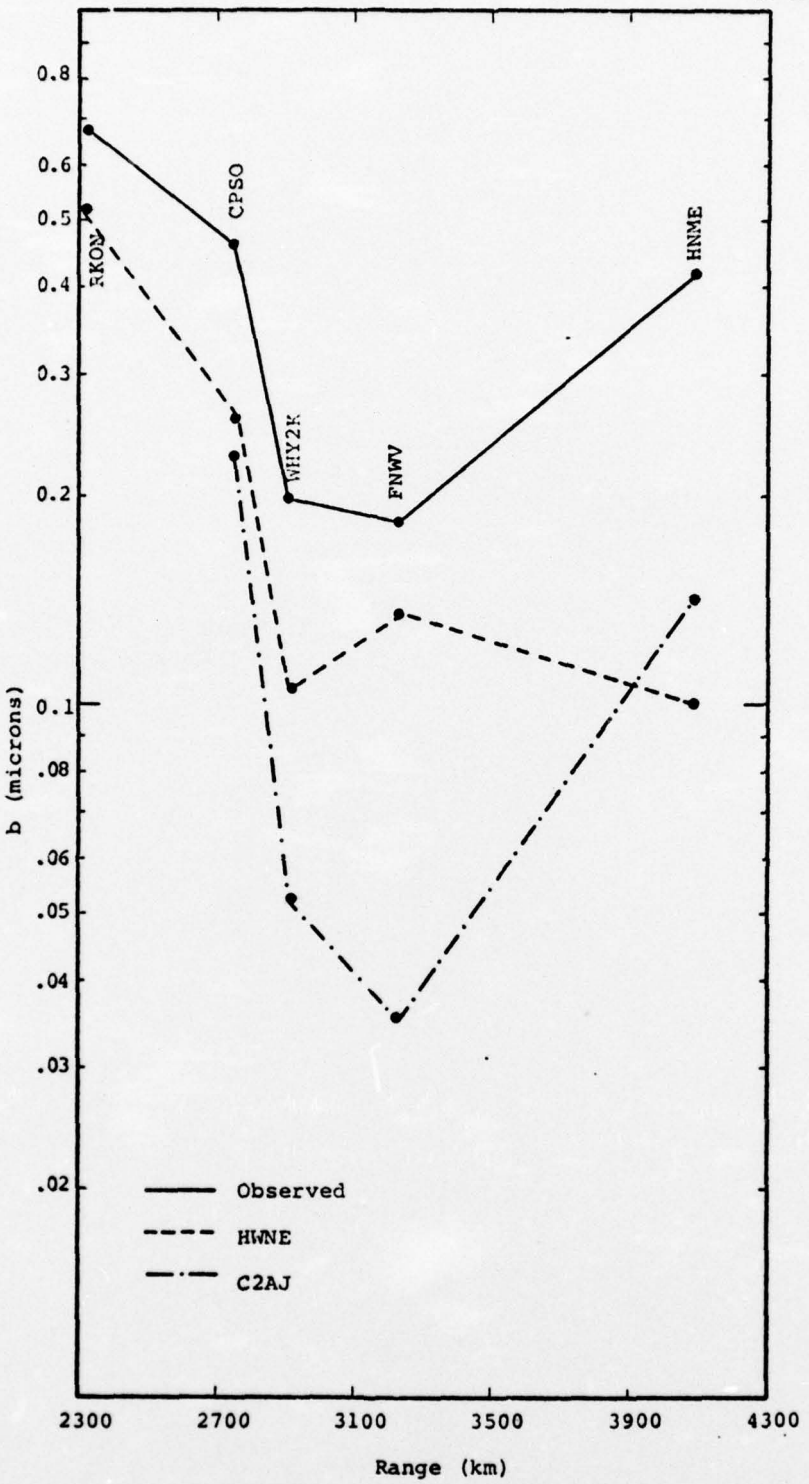

Figure 3.3. Initial comparison of observed and theoretical b amplitudes from seismograms in Figures 3.1 and 3.2. The amplitude in these and subsequent plots have been divided by the instrument magnification at the appropriate periods.

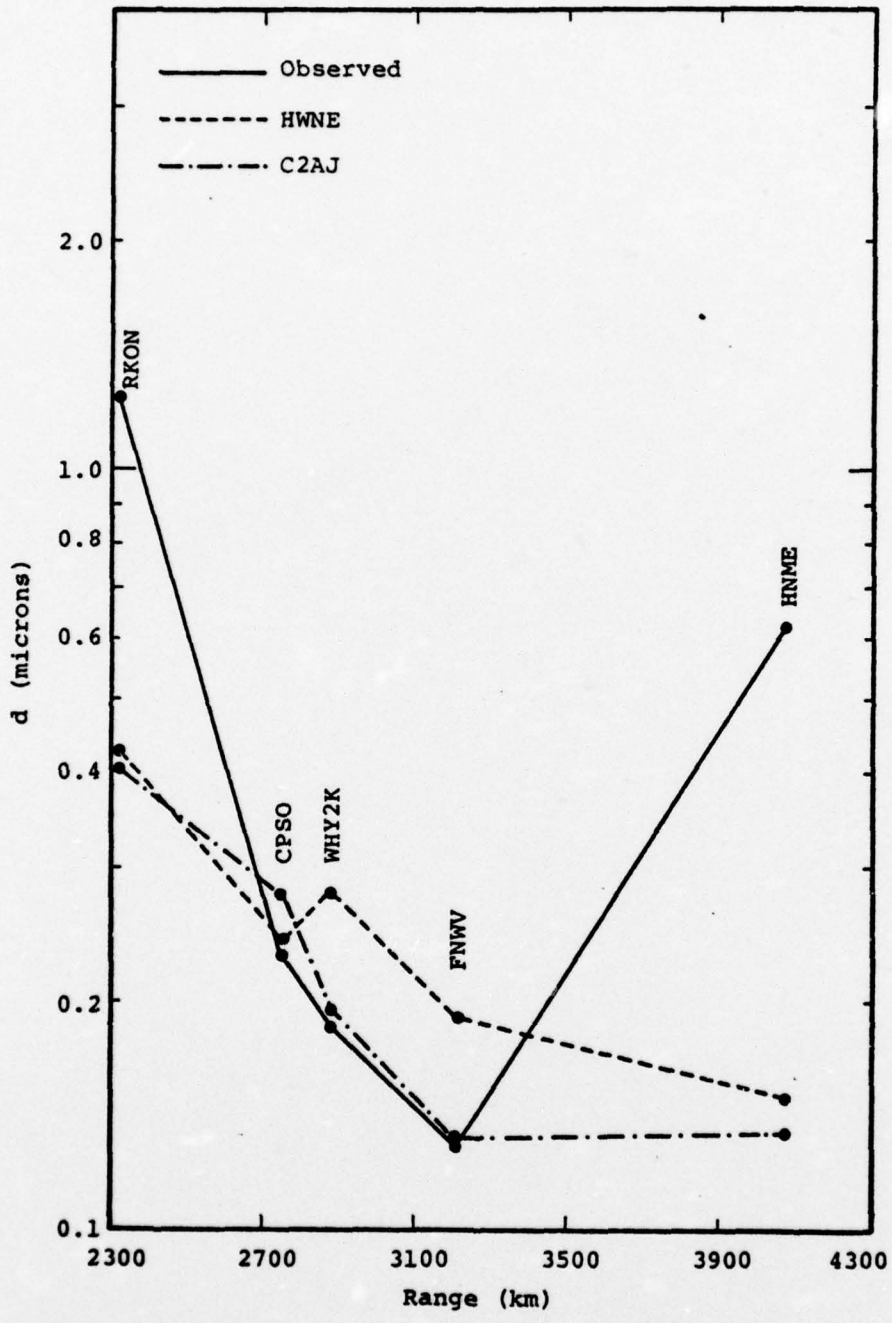

Figure 3.4. Comparison of observed and theoretical d amplitudes from Figures 3.1 and 3.2.

An effort was made to select an improved upper mantle model to give closer agreement between theory and observations. Implicit in this exercise is the assumption that the source and its vicinity is correctly modeled. A separate study (Bache, et al., 1975b) shows that such confidence is warranted.

The results of the more recent theoretical seismogram calculations are shown in Figs. 3.5 and 3.6 for two earth models: HWA-2 and HWNE-3 (shown in Figs. 3.9a and b). The amplitude comparisons for the b and d amplitudes are shown in Figs. 3.7 and 3.8. In our study of station characteristics (see Appendix A), the FNWV station was found to give amplitudes that are three times smaller than expected, irrespective of epicentral distance. Therefore, the observed amplitudes for FNWV plotted in Figs. 3.7 and 3.8 have been multiplied by the station correction factor of three.

The waveform comparisons for the new predictions, Figs. 3.5 and 3.6, are perhaps a bit better than for the initial predictions, Figs. 3.1 and 3.2. The shape of the seismograms and the maximum amplitude are not in good agreement at RKON and CPSO, however. The shape in the first few seconds at RKON and CPSO seems to be due to an interference between the initial arrival and a second arrival delayed by about one second. It appears that the second arrival is due to the upper mantle since the seismograms for LONG SHOT show no such complication. Attempts were made to simulate the RKON signal by perturbing published upper mantle models (HWA, HWB, HWNE, and C2AJ), but none were successful in fitting both travel time and amplitude data. A difficulty encountered in constructing new models was that the range sampling was too sparse. Such a sampling does not allow profiles to be constructed so that the amplitude and travel time behavior (the most useful diagnostics in inferring deep structure)

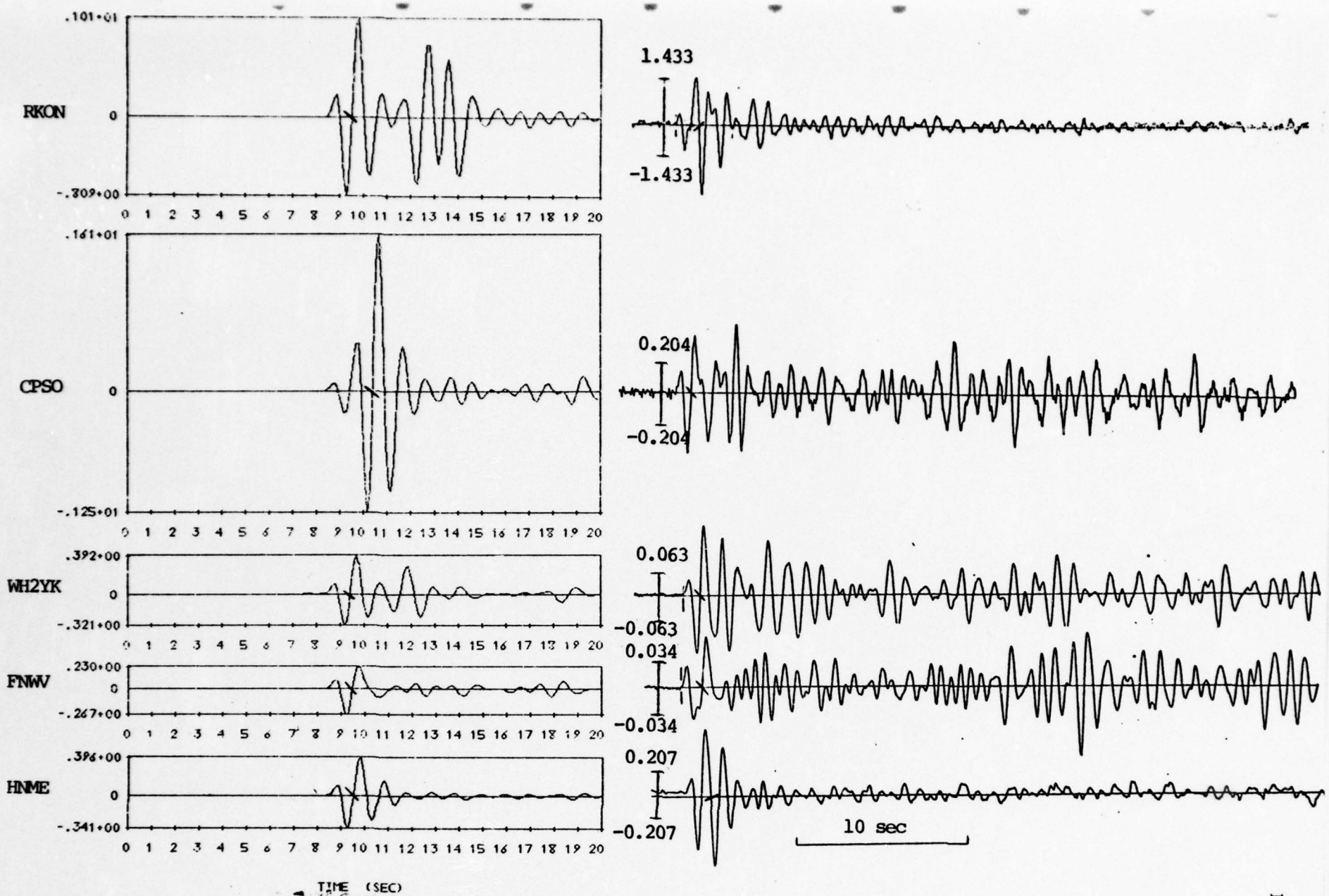

Figure 3.5. Short period vertical seismograms: observations on the right, and synthetics for the model HWA-2 on the left. The amplitude scale is indicated in microns at one Hz.

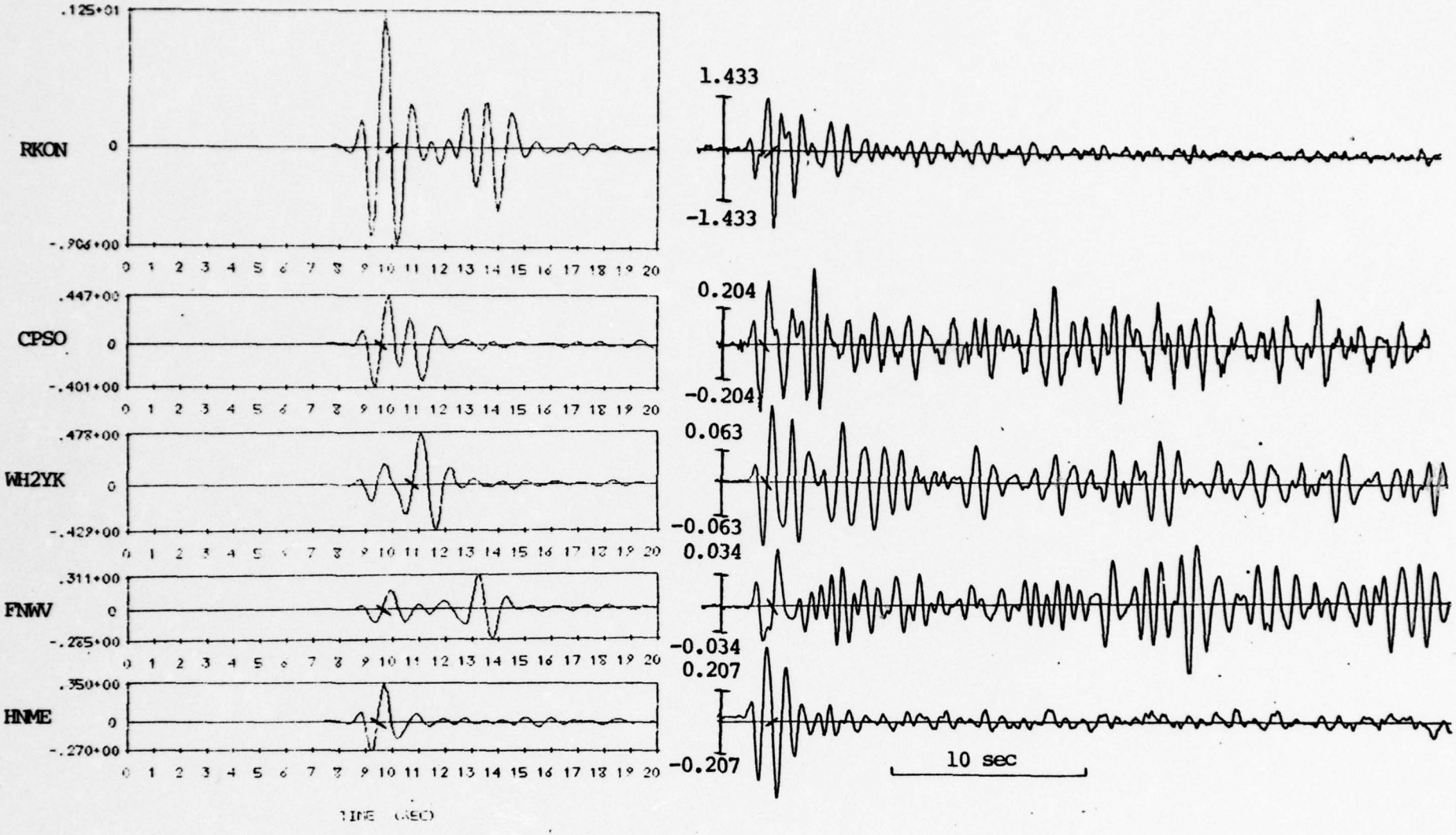

Figure 3.6. Short period vertical seismograms: observations on the right and synthetics for model HWNE-3 on the left. The amplitude scale is indicated in microns at one Hz.

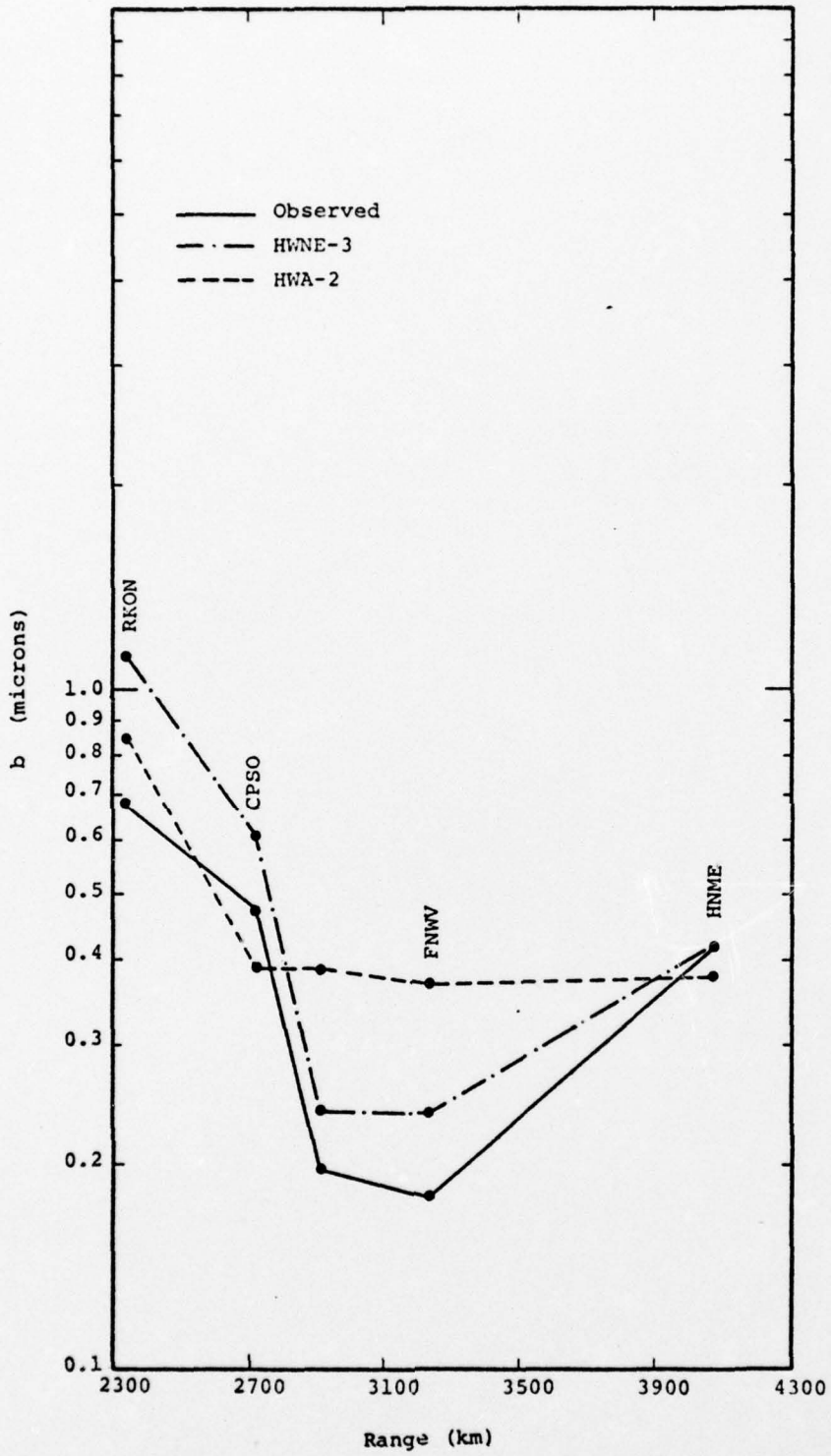

Figure 3.7. Revised comparison of observed and theoretical b amplitudes from the records of Figures 3.5 and 3.6.

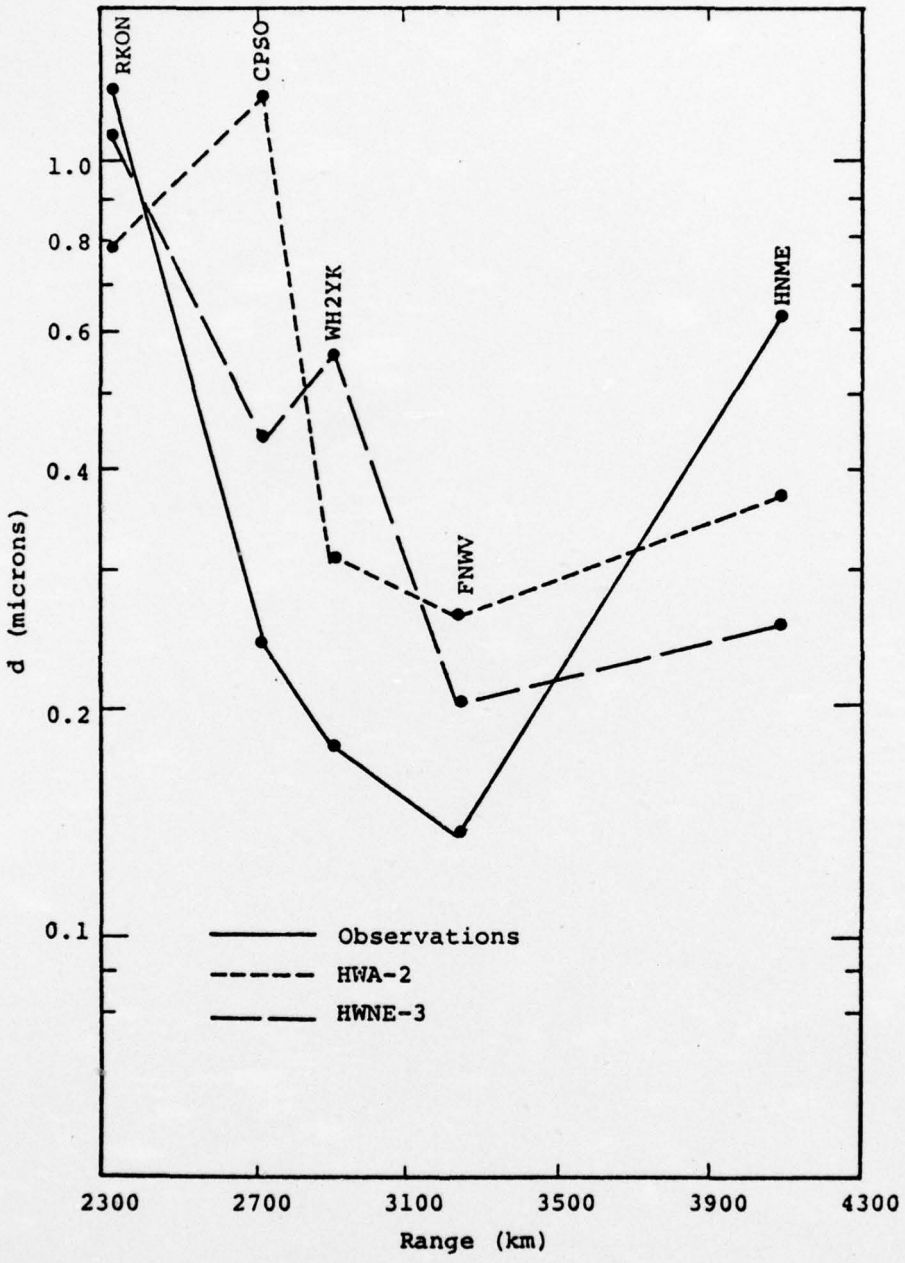

Figure 3.8. Revised comparison of predicted and observed d amplitudes from the records of Figures 3.5 and 3.6.

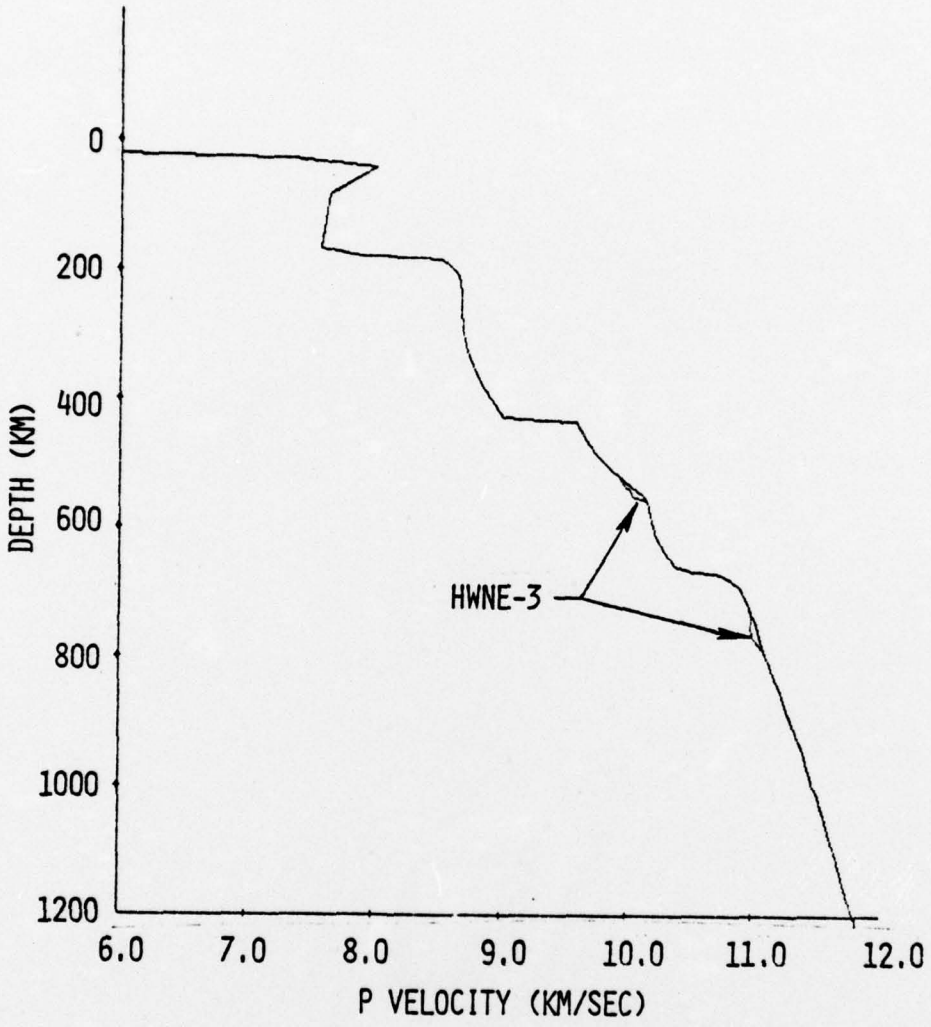

Figure 3.9a. Upper mantle models HWNE and HWNE-3.

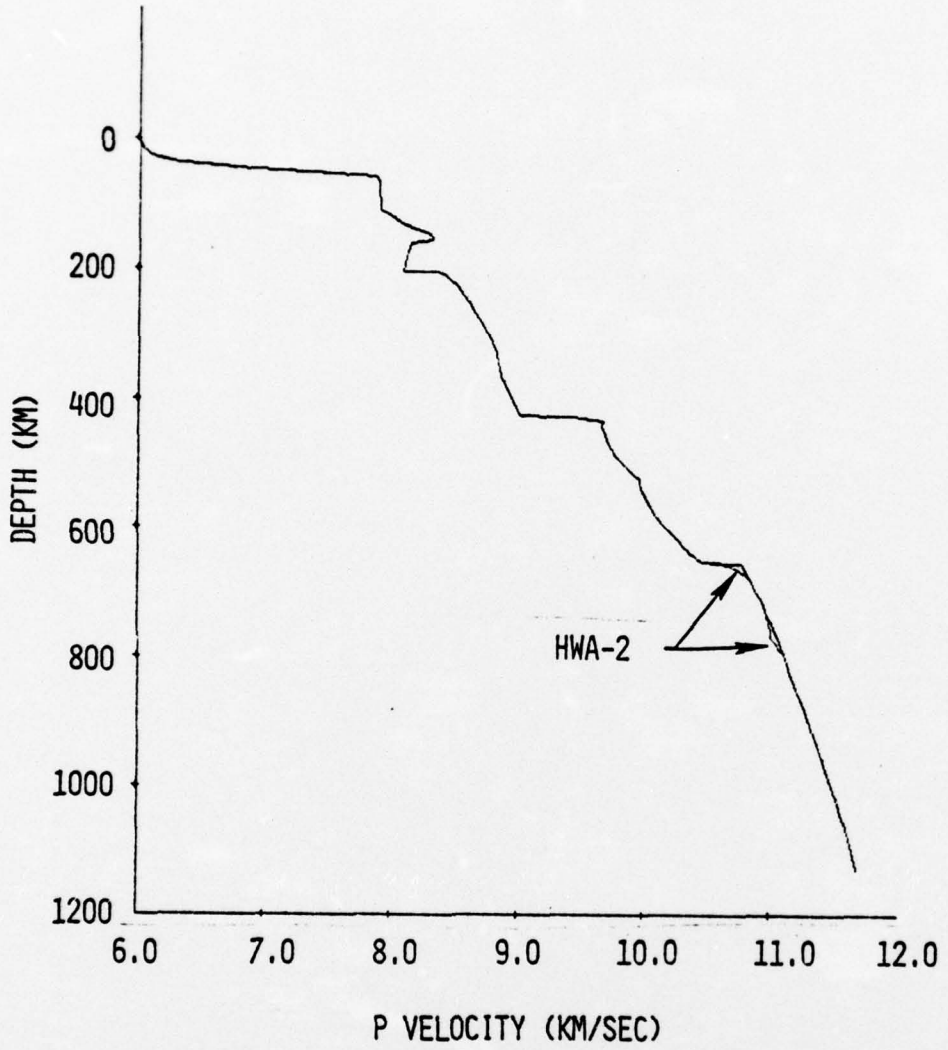

Figure 3.9b. Upper mantle models HWA and HWA-2.

are apparent. We are now trying to construct a data set consisting of several explosions and recordings at both LRSM and WWSS sites to rectify the difficulty. This should allow much better resolution of upper mantle models and make separation of mantle and crustal effects more clear.

It does appear that the factors controlling the amplitude of the b phase are properly included in the model. Evaluation of the predictions should rely most heavily on the b phase comparison since this phase is least affected by phenomena not related to the explosion coupling into elastic waves.

For the b amplitude the comparison (Fig. 3.6) between predicted and observed data is quite favorable, particularly for the HWNE-3 model. At several stations the two models span the observations. Taking HWNE-3 alone, the amplitudes are consistenly within 30-50 percent of the observations. For the d amplitude, the measurements are much more scattered, as might be expected.

3.5 COMPARISON BETWEEN THEORETICAL AND OBSERVED RAYLEIGH WAVES

As for body waves, comparison between observed and synthetic Rayleigh waves was made in two stages. The initial prediction was quite crude in that no serious attempt was made to select a propagation path model appropriate to each station. The earth model CIT109 (Archambeau, et al., 1969) was used for all stations. However, this model was deduced almost entirely from body wave observations and the surface layers are for an average shield path. In fact, this model was used mainly because it was computationally convenient at the time. The comparison between observed and synthetic waveforms and Airy phase amplitudes is shown in Figs. 3.10 and 3.11. This prediction was not particularly successful.

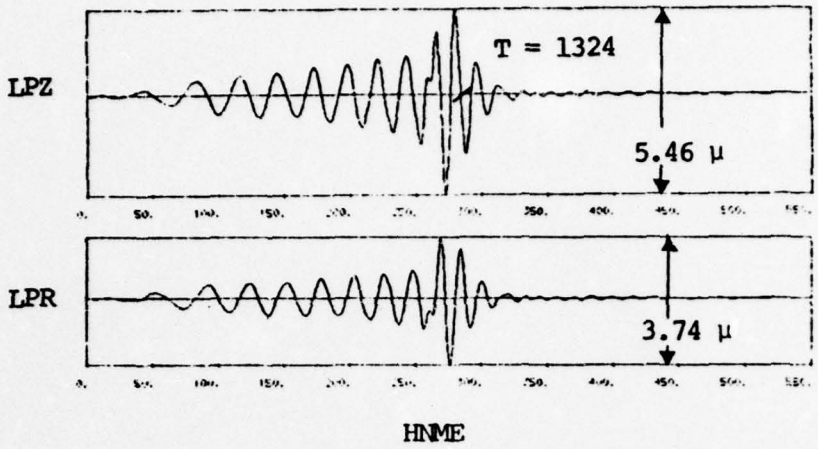

Figure 3.10. The theoretical long period record for HNME and the comparison of theoretical (left) and observed (right) long period data at RKON, CPSO, WHY2K and FNWV. The travel times, T, from detonation to the indicated zero crossing are given for all LPZ seismograms. The gain at 25 seconds period is indicated on each record. Both the vertical (LPZ) and radial (LPR) recordings are shown. For all synthetic seismograms the earth model CIT109 was used.

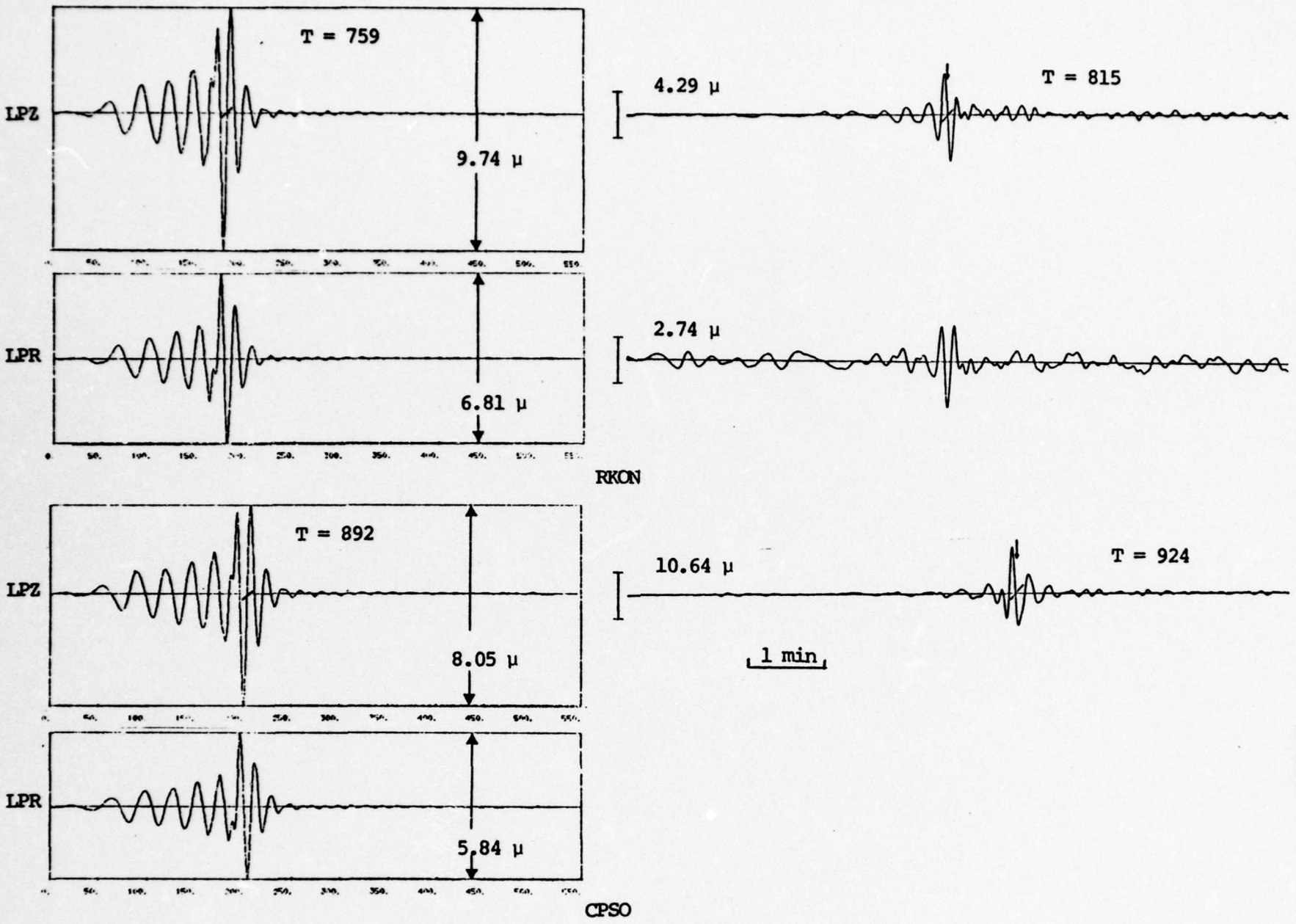

Figure 3.10 (Continued)

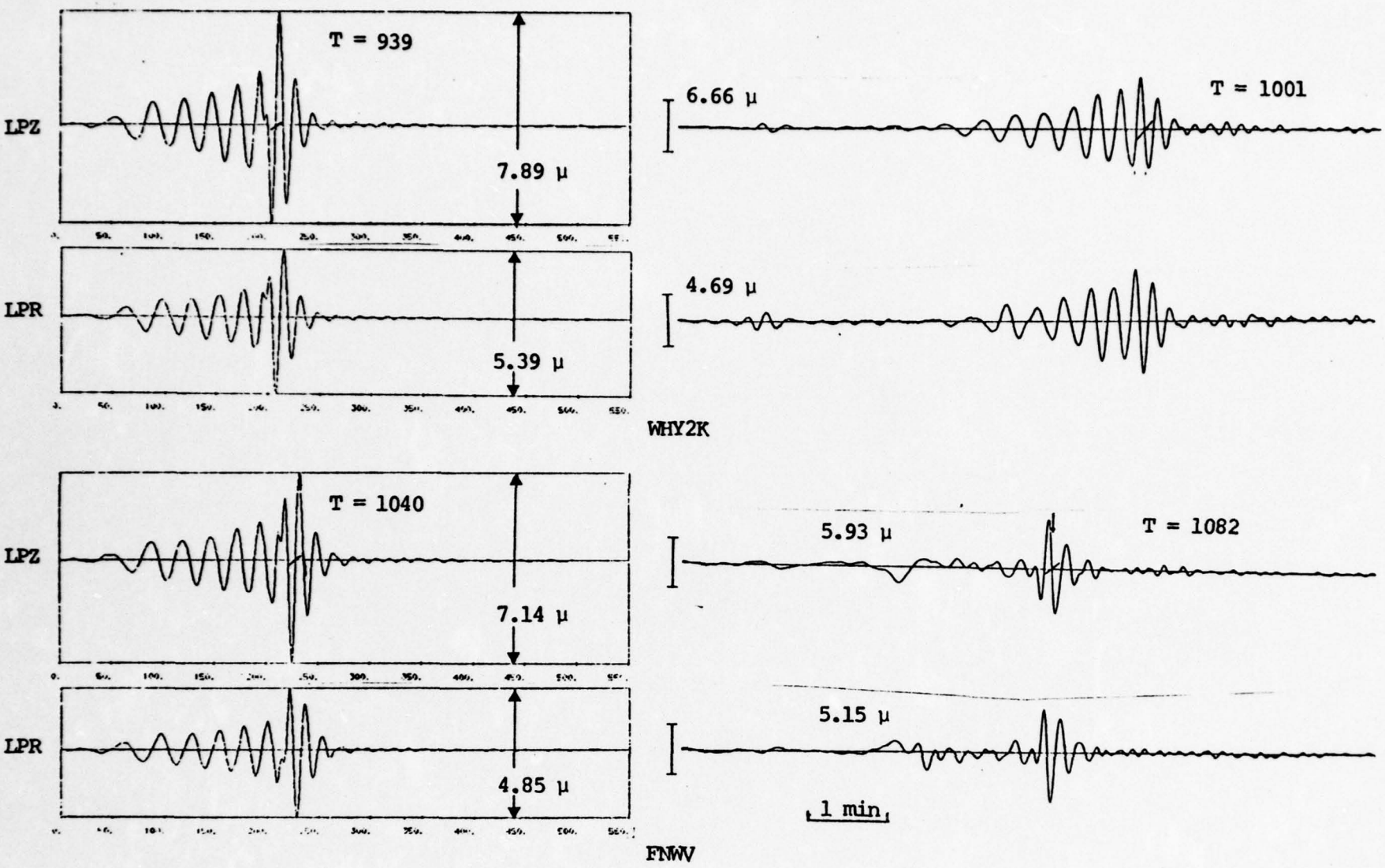

Figure 3.10 (Concluded)

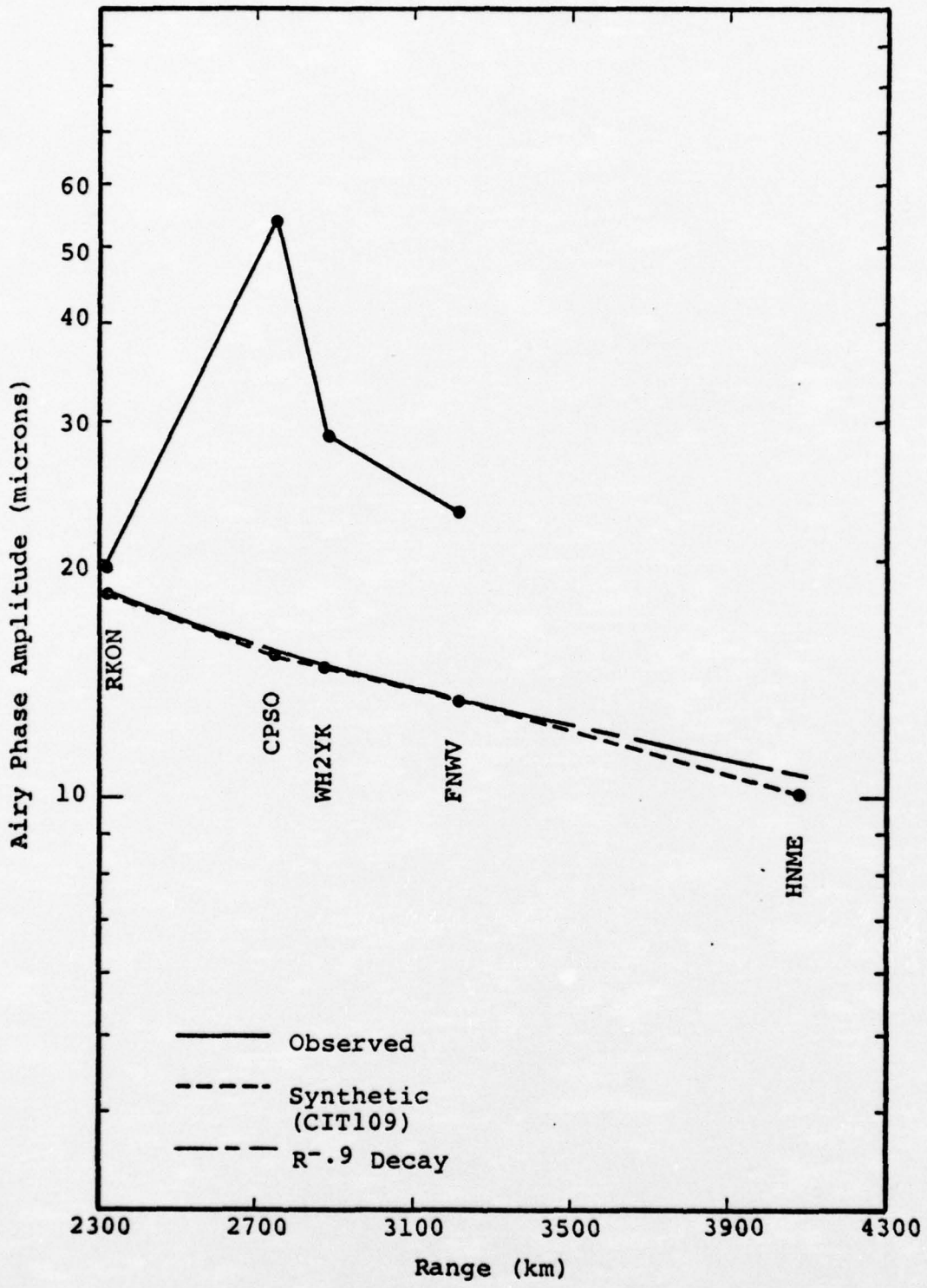

Figure 3.11. Initial comparison of observed and synthetic Airy phase amplitudes from the records of Figure 3.10.

For the revised theoretical seismograms a straightforward, but remarkably effective procedure was used. First, the S^3 data analysis program MARS (Bache, et al., 1975a; Savino, et al., 1975) was applied to the recorded MAST seismograms to determine the observed group velocity dispersion. The MARS program uses narrow band filter techniques to compute the dispersion curves. The results are shown in Fig. 3.12. While the MAST data was used at this stage, it is important to note that any earlier NTS event could have been used with no effect on the result. We have verified the fact that the group velocity dispersion curve at a given station is essentially independent of event.

Using the observed dispersion as a discriminator, a number of proposed earth models were examined to find those that seemed appropriate to each station. For WHY2K the model CIT109 was selected. For the other three stations a model deduced by McEvilly (1964) from central U.S. propagation paths was selected.

The earth models were then perturbed to cause the observed and theoretical group velocity curves and travel times to coincide. The new models, CIT109-A for WHY2K, MCEV-J for RKON and MCEV-B for CPSO and FNWV, are shown in Fig. 3.13 compared to the starting models. The dispersion curves for these models fit the observations to within 0.04 km/sec for periods between 10 and 30 seconds. The travel time fit is easily obtained by simply scaling all velocities by a constant, the changes amounting to a few percent at most. In fact, the model CIT109-A is the same as CIT109 except all velocities are multiplied by 1.06. The model MCEV-B resembles McEvilly's model in character, but MCEV-J is fairly different (the crustal low velocity zone has been removed). These models are not unique to the dispersion curves in Fig. 3.12, but do allow prediction of the observed time series.

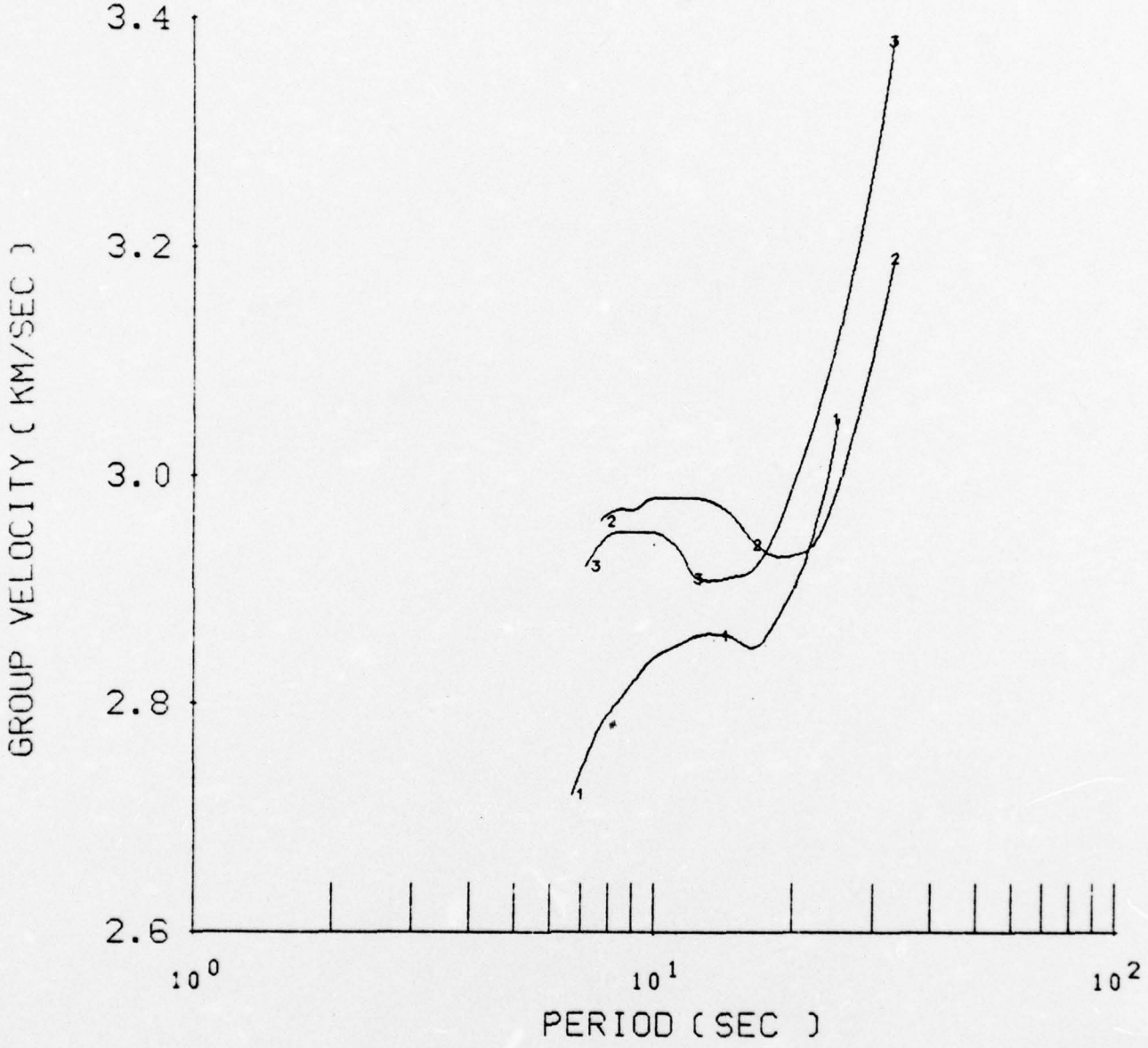

Figure 3.12. Observed dispersion curves for the MAST event at SDCS stations.

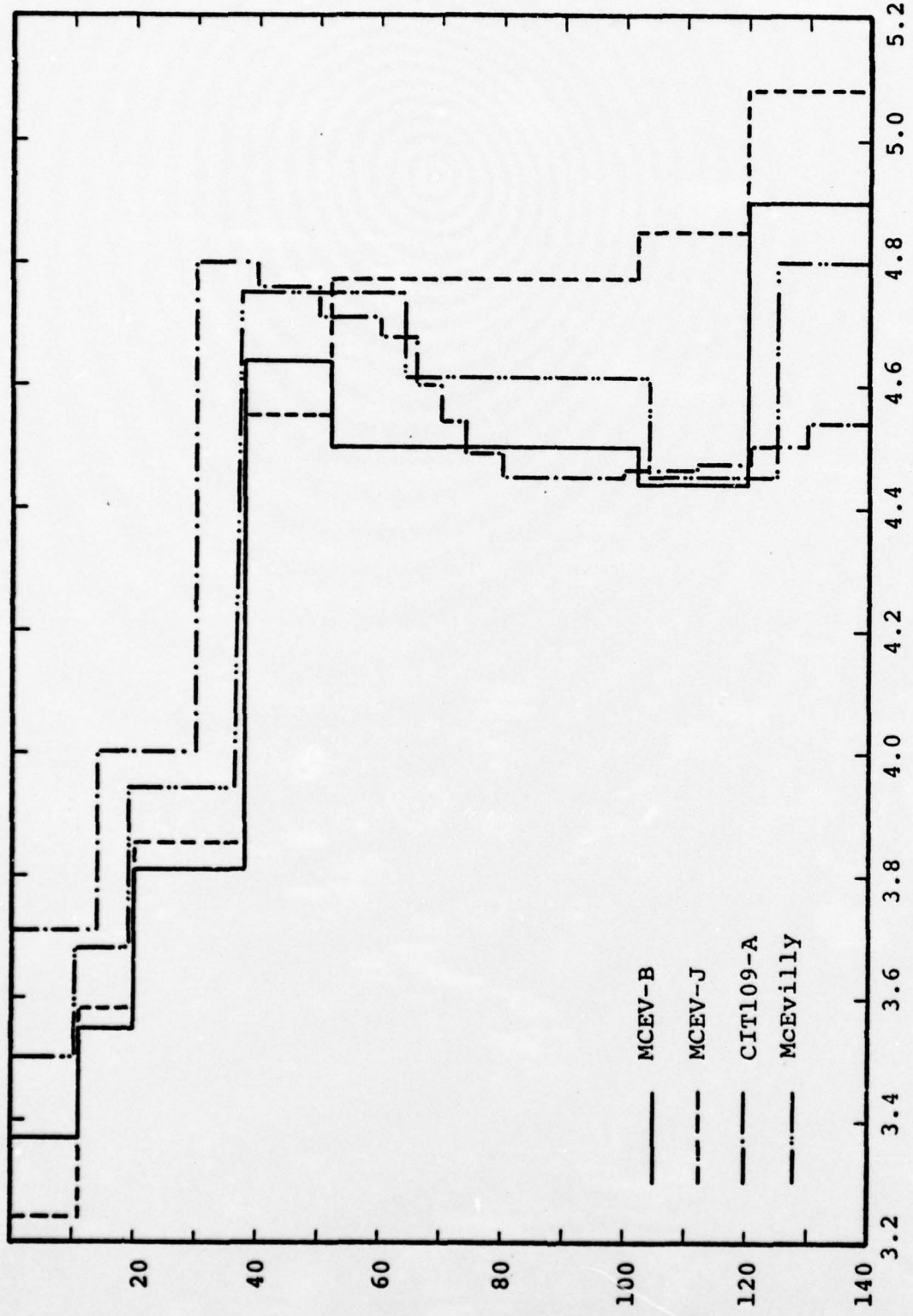

Figure 3.13. Crustal structures used in surface wave calculations.

To complete the earth model, values for the coefficients characterizing the observed anelastic attenuation are needed. The model proposed by Tryggvason (1965) was used.

The comparison between our final synthetic seismograms and the observed wave shapes and Airy phase amplitudes is shown in Figs. 3.14 and 3.15. The station HNME was not operating for MAST so it was not considered. The agreement between travel times and wave shapes is quite good, as expected.

The excellent agreement between observed and theoretical Airy phase amplitudes at three of the stations (Fig. 3.15) is quite gratifying. The other station, CPSO, will be discussed in some detail below. The important point is that we used published earth models deduced from a large body of data. We then modified the models slightly to include the peculiar dispersion and travel time characteristics of the particular source-receiver path. This can nearly always be done for a path of interest. The results give a great deal of confidence in our calculation of the long period level of the source.

Another interesting point concerns the errors introduced by different observers making amplitude-period measurements for the same seismic signals. This is indicated in Fig. 3.15. Two sets of amplitude measurements were made at S^3 and are plotted on this figure. For the first (open circles) the period of the measured phase was determined from seismograms which were included in the MAST shot report. These amplitudes correspond to those plotted in Fig. 3.11. The other set of observed amplitudes (solid line) was corrected for instrument response using the apparent periods given in the MAST shot report. The point is that the instrument correction varies rapidly in this period range and small differences have considerable effect on the amplitude (e.g., WH2YK).

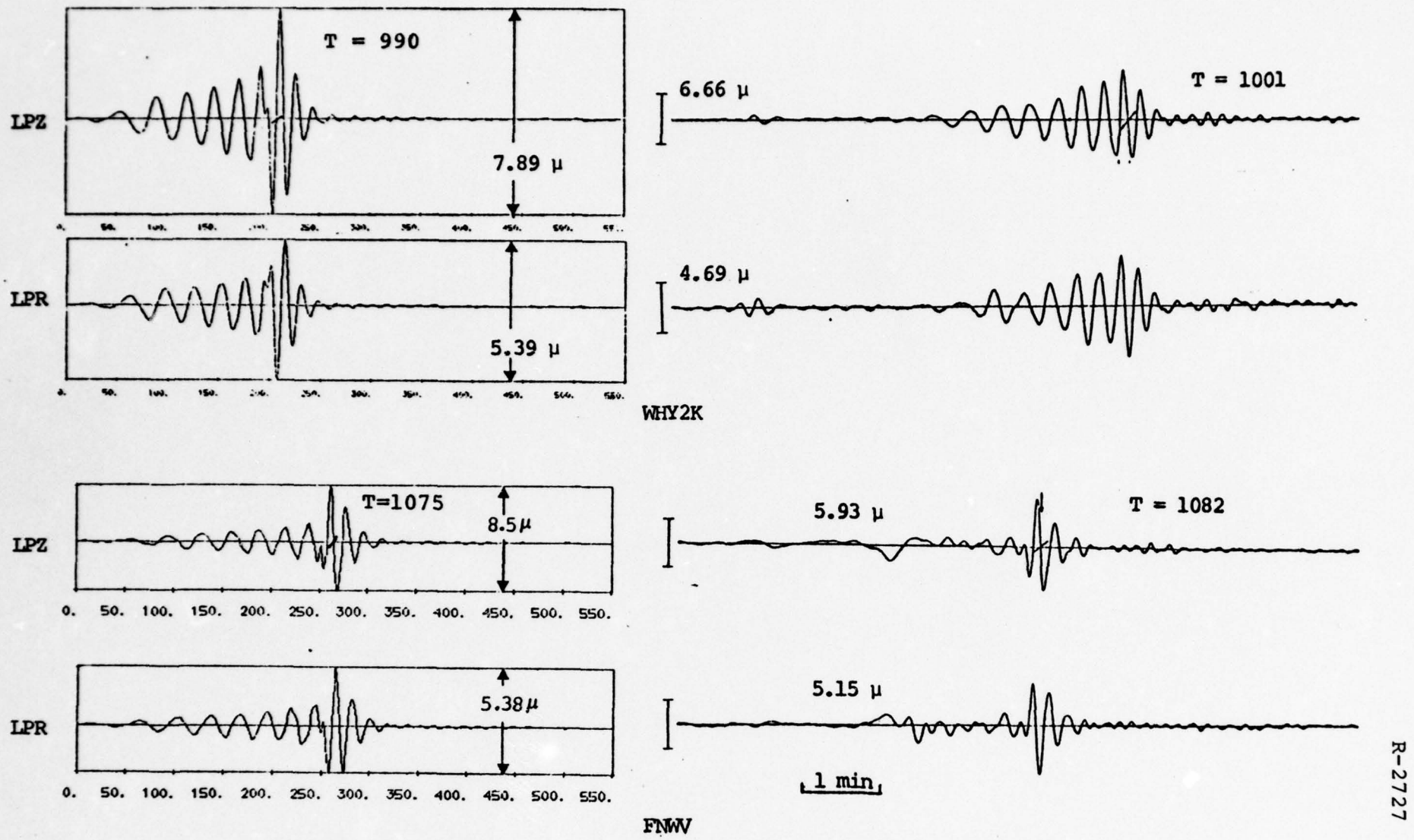

Figure 3.14. Revised theoretical (left) and observed (right) long period seismogram. The travel times, T, from detonation to the indicated zero crossing is indicated on each record. The gain at 25 sec is indicated on each record. Both the vertical (LPZ) and radial (LPR) recordings are shown.

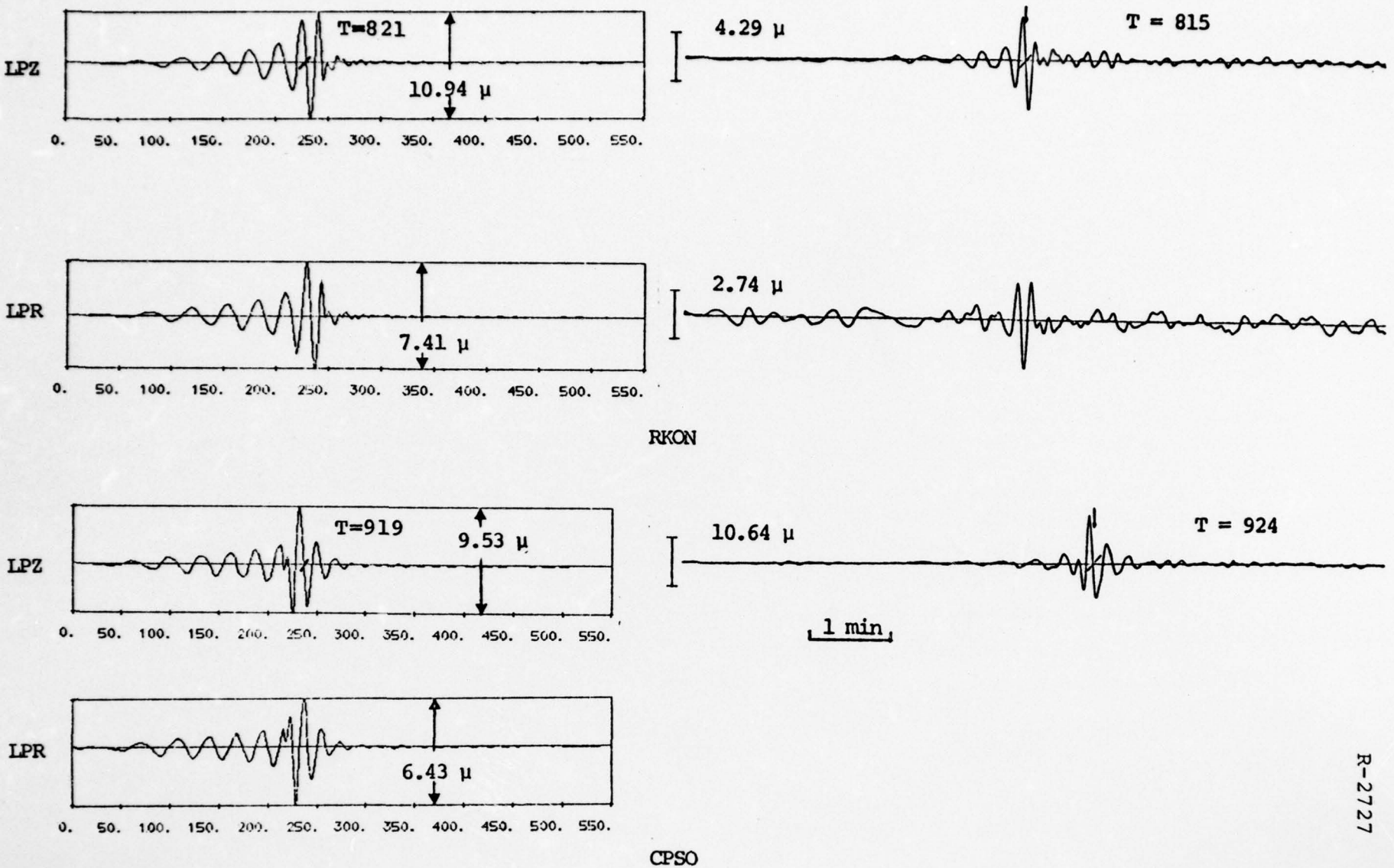

Figure 3.14 (Continued)

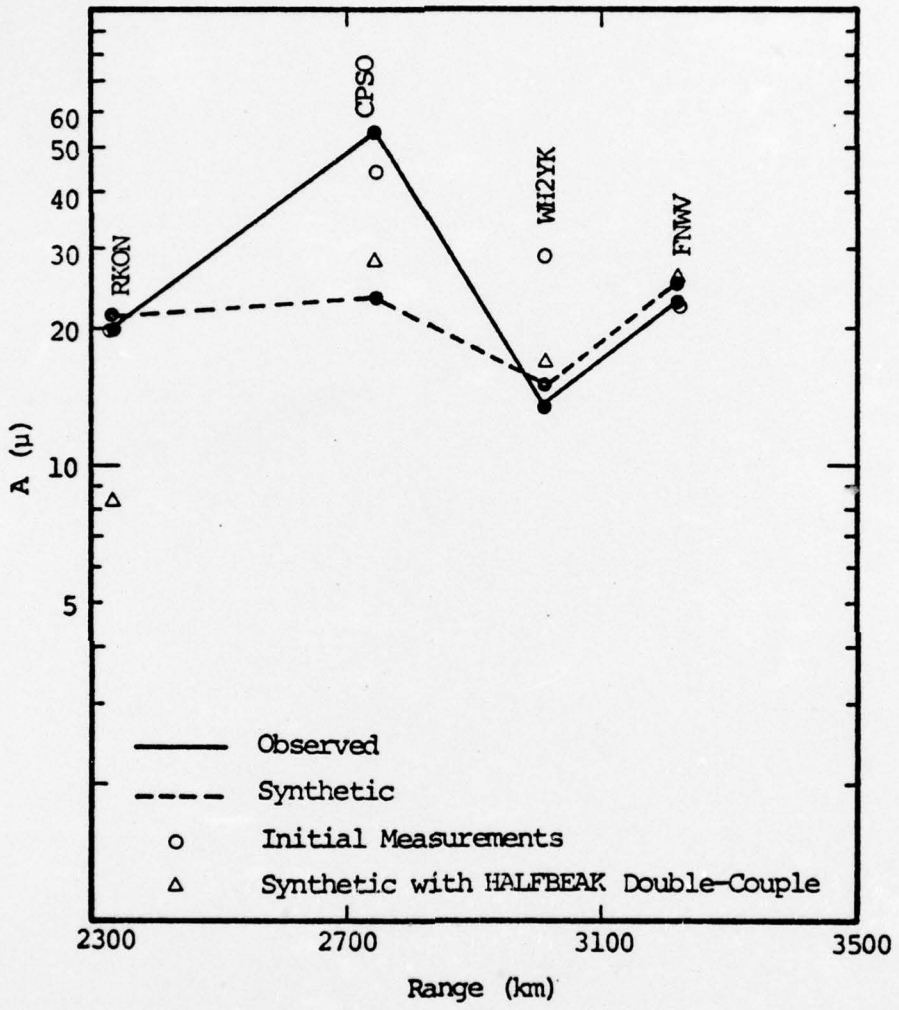

Figure 3.15. Revised comparison of observed and synthetic Airy phase amplitudes for the records of Figure 3.14.

There seems to be no simple explanation for the large amplitude at CPSO relative to RKON and FNWV. There are a number of possible causes that were not included in our modeling and we can speculate about the extent to which these may be responsible. Among these possible causes are radiation pattern effects associated with the source and lateral variations in the elastic and anelastic properties of the travel path.

First, we should relate these observations to previous experience with CPSO. Von Seggern (1973) analyzed some 686 Rayleigh wave amplitudes from North American LRSM recordings of 43 NTS explosions. Using a procedure he calls Joint Magnitude Determination, he fit these data to the unified distance relation*

$$\log A_{ij} = 4.25 - 0.90 \log r_{ij} + \hat{F}_j + \hat{C}_i,$$

where A is amplitude, r is epicentral distance, $\hat{F}_j$ is an event correction and $\hat{C}_i$ is a station correction. Using Von Seggern's $\hat{C}_i$, we can determine how stations at the SDCS sites have coupled on the average over the years. These data, normalized to the RKON amplitudes, are summarized in Table 3.3. From the table it is clear that relatively large amplitudes are commonly observed at CPSO. In passing, we also note that the MAST observation at WH2YK seems to be different from that expected from past experience.

To further delineate the past behavior of CPSO compared to RKON, we tabulate the relative amplitudes for a number of

*The distance decay as $r^{-.9}$ is almost precisely that predicted by our theoretical model when all factors but distance are held constant. This is indicated in Figure 3.11 and is due to the interaction between the elastic ($r^{-.5}$) and anelastic ($e^{-\gamma r}$) attenuation with distance.

TABLE 3.3

RELATIVE RAYLEIGH WAVE AMPLITUDES FOR MAST COMPARED TO AVERAGE VALUES FROM VON SEGGERN (1973)

Station	Epicentral Distance (degrees)	C_i	Average Relative Amplitude	MAST Relative Amplitude
RKON	21.02	-0.20	1.0	1.0
CPSO	24.74	0.17	2.0	2.7
WHY2K	26.18	0.12	1.7	0.7
FNWV	28.93	--	--	1.2

past events in Table 3.4. These values are taken from SDAC shot reports. Also given is the area in which the shot was detonated, the source material type and the yield from Springer and Kinnaman (1971). For these representative events the relative CPSO/RKON amplitude varies over a factor of two or more from the average value of 2.0 found by Von Seggern.

One possible explanation of the amplitude variation is that the scurce is not a symmetric radiator of Rayleigh waves but has a radiation pattern. In fact, a number of studied have concluded that the Rayleigh wave source does include a double-couple component (Lambert, et al., 1972; Toksöz and Kehrer, 1972; Aki and Tsai, 1972). This is usually attributed to the release of tectonic strain by the explosion.

Toksöz and Kehrer (1972) assumed that a double-couple of strike-slip orientation was imposed on the spherically symmetric source. Using Rayleigh and Love wave data, they then obtained best fit values for the strength, F, and orientation, $\theta_{D.C.}$, of the double couple. These values are tabulated in Table 3.5 for each explosion for which they are available. Now, if the double-couple orientation were more or less the same from event to event, station amplitudes would vary from radiation pattern effects alone and Von Seggern's $\hat{C}_i$ could be merely a radiation pattern correction. In fact, the orientation obtained by Toksöz and Kehrer is in the 330°-355° range for 15 of the 18 NTS events studied.

The Rayleigh wave enhancement $(1 + F \sin 2(\theta-\theta_0)$, θ being the azimuth of the station from the source and θ_0 the orientation of the double couple) due to the best fit double-couple source found by Toksöz and Kehrer is indicated in Table 3.5. It is clear that the superposition of this double-couple generally acts to suppress the amplitude at RKON and to enhance that at CPSO. This is not surprising since the CPSO/RKON ratios previously indicated in Table 3.4 were among the data used to fit the double-couple source.

TABLE 3.4

RELATIVE RAYLEIGH WAVE AMPLITUDES (CPSO/RKON)
FOR A NUMBER OF NTS EXPLOSIONS

Event	Type	Yield	Relative Amplitude
PILEDRIVER	Granite	≈56	1.8
CHARTREUSE	Pahute Mesa Rhyolite	70	2.2
HALFBEAK	Pahute Mesa Rhyolite	300	3.5
GREELEY	Pahute Mesa Tuff	825	2.7
CUP	Yucca Flat Tuff	L-I	1.2
BILBY	Yucca Flat Tuff	235	3.7
BRONZE	Yucca Flat Tuff	L-I	1.4
COMMODORE	Yucca Flat Tuff	250	2.1
DUMONT	Yucca Flat Tuff	L-I	4.4

TABLE 3.5

RAYLEIGH WAVE ENHANCEMENT BY SUPERPOSITION OF A DOUBLE-COUPLE ON THE MONOPOLE EXPLOSION SOURCE

Event	F	$\theta_{D.C.}$	RKON	CPO	WHY2K	FNWV
PILEDRIVER	3.2	340°	-1.6	2.6	1.1	1.7
CHARTREUSE	0.9	353°	0.1	1.1	0.8	1.4
HALFBEAK	0.67	345°	0.4	1.2	1.0	1.1
GREELEY	1.6	355°	0.6	1.0	1.8	0.5
CUP	0.55	200°	0.6	0.6	1.5	0.5
BILBY	0.47	340°	0.6	1.2	1.1	1.1
BRONZE	0.33	185°	0.7	0.9	1.3	0.8

The double-couple source causes the amplitudes of the other stations (WHY2K and FNWV) to change by varying amounts. Certainly if this effect occurs, failure to account for it can cause amplitude errors of a factor of two or even more at individual stations.

What is the meaning of this discussion of tectonic release for the MAST predictions of this report? We haven't enough data to estimate the F, $\theta_{D.C.}$ for this event. However, MAST is quite similar to HALFBEAK. If the HALFBEAK double-couple from Table 3.5 were added to the explosion source used here, the predicted amplitudes would be altered by approximately the factors given in the table. These altered amplitudes are indicated by the open triangles on Figure 3.15. The fit would be a great deal worse for RKON, slightly better for CPSO and unchanged for WHY2K and FNWV. For the $\theta_{D.C.}$ selected, RKON occurs near a node and so is quite sensitive to this value. With this in mind, it seems fair to say that the validity of our predictions is not compromised by failure to include tectonic release. Before leaving the subject, it should also be noted that the effect of tectonic release on the body waves is almost certainly negligible (see Bache, 1976).

There are other effects not included in our models which can also cause amplitude variations. First, the same dissipation model has been used for all paths. However, this is a weak effect that seems unlikely to account for even a factor of two for this set of stations (for a recent summary of the data see Herrmann and Mitchell, 1975). Certainly stations like FNWV and CPSO must have nearly the same path attenuation since their azimuths vary by only 8°.

Another possibility is lateral refractors. McGarr (1969) demonstrates that large amplitude variations between stations at very nearly the same azimuth are possible due to

focusing and defocusing of surface waves by lateral heterogeneities. In addition, near receiver structures can cause amplitude variation if their size is on the order of the surface wave wavelengths ($\sim$ 50 km). These two mechanisms can leave dispersion curves nearly unchanged since the group delays caused by the localized structures are small compared to those of the major part of the path. Shown in Figure 3.16 are the amplitude data for a line of stations on the same azimuth for the LONG SHOT and RULISON events (data from shot reports). The scatter around a simple $R^{-.5}$ or $R^{-.9}$ dependence is indicative of the variations possible even when the azimuth is held fixed.

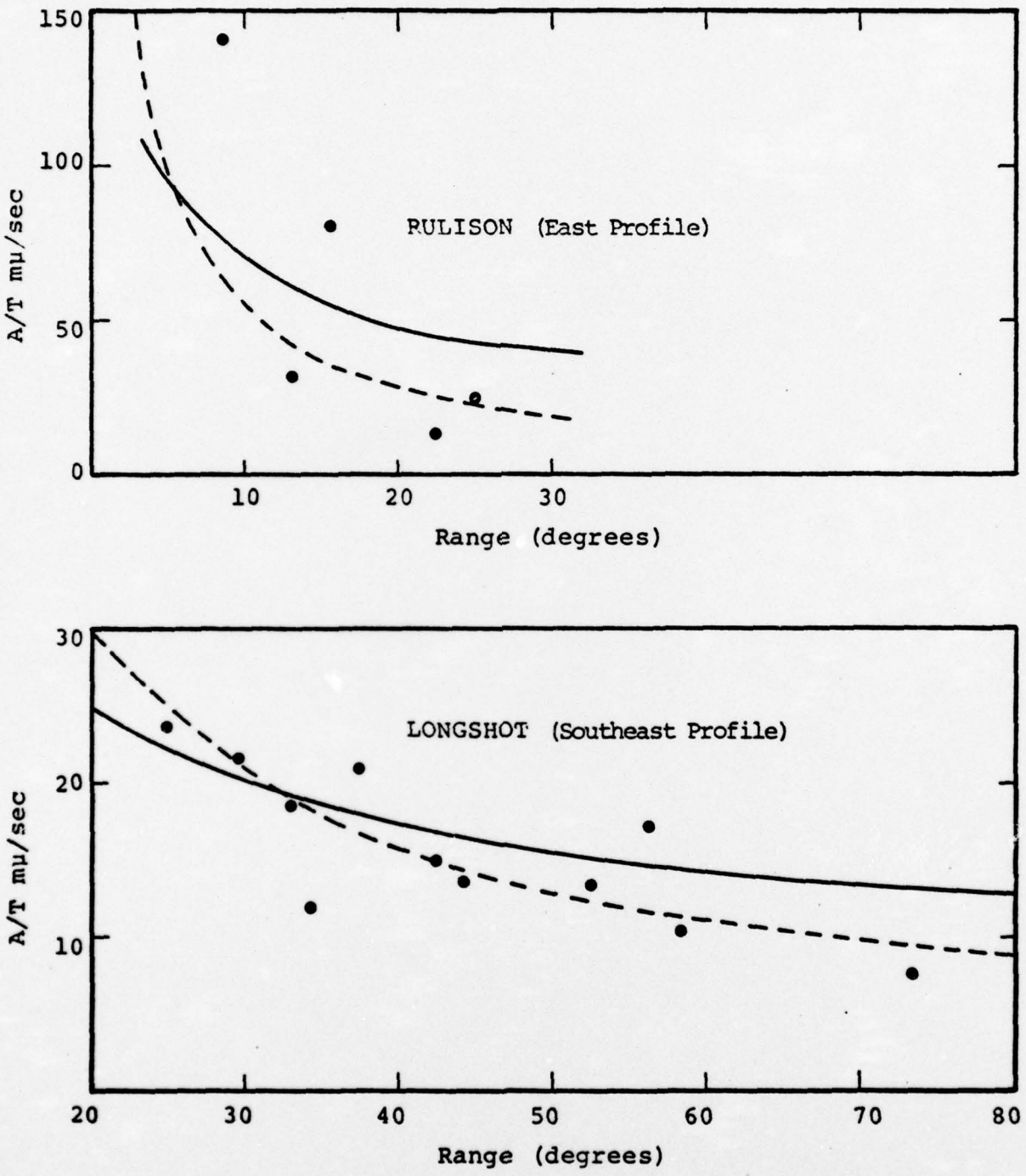

Figure 3.16. Observed surface wave amplitudes for stations along a fixed azimuth. Solid and dashed line indicate $R^{-.5}$ and $R^{-.9}$ decay, respectively.

IV. SUMMARY AND CONCLUSIONS

For making seismogram predictions there are three elements that must be dealt with: (1) the wave produced by the source; (2) the average travel path; (3) the properties peculiar to the receiver region. Important features of each of these elements as handled here are summarized below.

The Source

- Material properties and constitutive models that were determined from preshot data were used in the RDP calculation.
- For the predictions the source was considered to be a spherically symmetric radiator of elastic waves.

The Travel Path

- For both body and surface waves, average earth models taken from the literature give reasonably good predictions of teleseismic amplitude, at least averaged over a number of stations.
- The single station waveform and amplitude match can be considerably improved by constructing average models that are specific to the source-receiver pair.
- Only those effects that can be represented by laterally homogeneous horizontally layered models were included in the calculations.
- For surface waves the earth models can easily be adjusted to match the actual dispersion characteristics of the travel path. The predicted wave shapes then match the observed quite closely.
- For stations within the triplication range, it is very difficult to construct earth models that accurately reproduce the complicated phase interference observed on the short period records.

- Amplitude predictions of body waves are best judged by the b phase prediction. This is especially true within the triplication range.

The Receiver Region

- Site corrections can and should be determined to represent local effects quite difficult to include in the models.
- Horizontal layered models of the receiver region are of little use for explaining the local effects observable on the short period records.

The theoretical amplitudes match the observed to much closer than a factor of two for nearly every short and long period (vertical) observation. The final comparisons are shown in Figures 3.7 and 3.15. Tables 4.1 and 4.2 summarize body and surface wave magnitude* data using the amplitudes in Figures 3.7, 3.8 and 3.15. With the experience gained in this exercise, preshot predictions of future events recorded at these stations may be done with nearly this accuracy.

*Surface wave magnitudes were computed using the tables in Marshall and Basham (1972), using the path correction P(T) for continental North America. Body wave magnitudes used distance corrections from SDAC shot reports.

TABLE 4.1

BODY WAVE MAGNITUDE FOR MAST COMPUTED FROM OBSERVED AND SYNTHETIC (HWNE-3) SEISMOGRAMS

Station	b(mμ)	T_b	A(½p-p)	T_A	Distance Correction B	m_b'	m_b
RKON (OBS)	680	0.70	1200	0.7	3.1	6.1	6.3
(SYN)	1180	0.96	1077	1.0		6.2	6.1
CPSO (OBS)	459	0.90	230	0.8	3.5	6.2	6.0
(SYN)	597	0.94	424	1.0		6.3	6.1
WH2YK (OBS)	193	1.0	170	1.2	3.4	5.7	5.6
(SYN)	222	0.92	559	1.1		5.8	6.1
FNWV (OBS)	162	0.96	120	(1.0)	3.6	5.8	(5.7)
(SYN)	215	1.02	185	1.1		5.9	5.8
HNME (OBS)	414	0.80	630	1.2	3.5	6.2	6.2
(SYN)	422	0.96	247	0.9		6.1	5.9

Note: $m_b = \log\left(\frac{A}{T_A}\right) + B$ and $m_b' = \log\left(\frac{b}{T_b}\right) + B$.

TABLE 4.2

SURFACE WAVE MAGNITUDES FOR MAST COMPUTED FROM OBSERVED AND SYNTHETIC SEISMOGRAMS

Station	A(μ)(½p-p)	T	Distance Correction B	Path Correction P(T)	m_s
RKON (OBS)	9.9	14.0	1.27	-0.46	4.8
(SYN)	10.6	14.4		-0.43	4.9
CPSO (OBS)	27.0	15.0	1.34	-0.38	5.4
(SYN)	11.7	14.0		-0.46	5.0
WH2YK (OBS)	6.7	17.0	1.36	-0.24	5.0
(SYN)	7.4	14.0		-0.46	4.8
FNWV (OBS)	11.6	16.0	1.41	-0.30	5.2
(SYN)	12.5	14.8		-0.40	5.1

Note: $m_s = \log (A) + B + P(T)$.

V. REFERENCES

Aki, K. and Y. Tsai, "The Mechanics of Love Wave Excitation by Explosive Sources," J. Geophys. Res., 77, 1972.

Archambeau, C. B., E. A. Flinn, and D. G. Lambert, "Fine Structure of the Upper Mantle," J. Geophys. Res., 74, 5825-5865, 1969.

Bache, T. C., J. T. Cherry, K. G. Hamilton, J. F. Masso, and J. M. Savino, "Application of Advanced Methods for Identification and Detection of Nuclear Explosions from the Asian Continent," Systems, Science and Software Report SSS-R-75-2646, May 1975a.

Bache, T. C., J. T. Cherry, N. Rimer, J. M. Savino, T. R. Blake, T. G. Barker, and D. G. Lambert, "An Explanation of the Relative Amplitudes of the Teleseismic Body Waves Generated by Explosions in Different Test Areas at NTS," Systems, Science and Software Final Report for DNA, October 1975b.

Bache, T. C., "The Effect of Tectonic Release on Explosion P Wave Signatures," submitted to Bull. Seism. Soc. Amer., 1976.

Cherry, J. T., N. Rimer, and W. O. Wray, "Seismic Coupling from a Nuclear Explosion: The Dependence of the Reduced Displacement Potential on the Nonlinear Behavior of the Near Source Rock Environment," Systems, Science and Software Report SSS-R-76-2742, September 1975a.

Cherry, J. T., N. Rimer, J. M. Savino, and W. O. Wray, "Improved Yield Determination and Event Identification Research," Systems, Science and Software Report SSS-R-75-2696, August 1975b.

Garg, S. K., "Constitutive Equations for Fluid-Saturated Porous Media," Systems, Science and Software Report SSS-R-76-2766, October 1975.

Garg, S. K. and A. Nur, "Effective Stress Laws for Fluid Saturated Porous Rocks," J. Geophys. Res., 78, 1973.

Harkrider, D. G., "Surface Waves in Multilayered Media. I. Rayleigh and Love Waves from Sources in a Multilayered Half-Space," Bull. Seism. Soc. Amer., 54, 627-679, 1964.

Harkrider, D. G., "Surface Waves in Multilayered Elastic Media. II. Higher Mode Spectra and Spectral Ratios from Point Sources in Plane Layered Earth Models," Bull. Seism. Soc. Amer., 60, 1937-1988, 1964.

Haskell, N. A., "Crustal Reflection of Plane P and SV Waves," J. Geophys. Res., 72, 2583-2587, 1962.

Helmberger, D. V. and R. A. Wiggins, "Upper Mantle Structure of the Midwestern United States," J. Geophys. Res., 76, 3229-3245, 1971.

Herrman, R. B. and B. J. Mitchell, "Statistical Analysis and Interpretation of Surface-Wave Anelastic Attenuation for the Stable Interior of North America," Bull. Seism. Soc. Am., 65(5), 1975.

Hill, P. and C. Pakiser, "Seismic-Refraction Study of Crustal Structure Between the Nevada Test Site and Boise, Idaho," Geol. Soc. of Amer. Bull., 78, 685-704, 1967.

Marshall, P. D. and P. W. Basham, "Discrimination Between Earthquakes and Underground Explosions Employing an Improved M_S Scale," Geophys. J. Roy. Astr. Soc., 28, 1972.

McEvilly, T. V., "Central U.S. Crust - Upper Mantle Structure from Love and Rayleigh Wave Velocity Inversion," Bull. Seism. Soc. Am., 54(6), 1964.

McGarr, A., "Amplitude Variations of Rayleigh Waves - Horizontal Refractions," Bull. Seism. Soc. Am., 59(3), 1969.

Savino, J. M., T. C. Bache, J. T. Cherry, K. G. Hamilton, D. G. Lambert and J. F. Masso, "Application of Advanced Methods for Identification and Detection of Nuclear Explosions from the Asian Continent," Systems, Science and Software Report SSS-R-76-2792, December 1975.

Springer, D. L. and R. L. Kinnaman, "Seismic Source Summary for U.S. Underground Nuclear Explosions," Bull. Seism. Soc. Am., 64, 1974.

Toksöz, M. N. and H. H. Kehrer, "Tectonic Strain Release by Underground Nuclear Explosions and Its Effect on Seismic Discrimination," Geophys. J. Roy. Astr. Soc., 31, 1972.

Tryggvason, E., "Dissipation of Rayleigh Wave Energy," J. Geophys. Res., 70(6), 1965.

von Seggern, D., "Joint Magnitude Determination and Analysis of Variance for Explosion Magnitude Estimates," Bull. Seism. Soc. Am., 63(3), 1973.

Wiggins, R. A. and D. V. Helmberger, "Upper Mantle Structure of the Western United States," J. Geophys. Res., 78, 1870-1888, 1973.

Wiggins, R. A. and D. V. Helmberger, "Synthetic Seismogram Computation by Expansion in Generalized Rays," Geophys. J. Roy. Astr. Soc., 37, 73-90, 1974.

APPENDIX A

SITE EVALUATION AND CORRECTION

The ideal station from our point of view would be situated such that teleseismic wave fronts are not distorted by the crust beneath the station or by the coupling of the seismometer to the crust. Before good comparisons between synthetic seismograms and data recorded at a certain site can be made, it is important to estimate that site's departure from ideal, and to correct the synthetic seismograms accordingly. We have used three criteria in determining whether a station is a "good" (close to ideal) station:

1. The ratio, R_{TZ}, of the maximum amplitude in the first few cycles of tangential motion to the same measure of vertical motion. The ratio should be small (< 0.2, say), indicating that a small amount of P energy was converted to SH. SH energy propagated from the source should arrive much later. SH motion near the onset of the seismogram indicates P to SH conversion by non-parallel interfaces or scattering.

2. The duration, T_c, of the coda. Although it is generally not necessary to quantify the estimate of T_c since a visual inspection will suffice, one might define T_c as the time required for running mean (of duration $\sim$ 5 sec) to decay to a certain level. Large values of T_c indicate internal reflections and scattering.

3. The ratio, R_A, of amplitudes recorded at stations beyond upper mantle triplications. At ranges beyond 40° (and less than 100° where the core introduces complications) the amplitude should be nearly proportional to R^{-1}. Variations from

R^{-1} spreading can be taken to be due to differences in the station coupling. Therefore, a station correction, C_s, can be deduced from the ratios, R_A, corrected for R^{-1} spreading.

The most satisfying means for dealing with stations which are poor in the above sense is to infer the physical process which is responsible and include that process in our analysis. To this end we have attempted to determine whether plane layering in the receiver crust can produce appreciable distortion of the pulse (see Appendix B). We find that plane layered models are unlikely to account for the observed distortion. Also, plane layering cannot be responsible for P or SV to SH conversion. We have not yet investigated other possibilities.

For the seismogram stations of interest in this report, the R_{TZ}, T_C and C_s for the criteria 1-3 discussed above have been computed and are tabulated in Tables A.1-A.3. For R_{TZ} and T_C observations of the MAST event were used. We are presently looking at observations of other events to verify the fact that these are not significantly influenced by peculiarities of the event. For the station correction, C_S, the following procedure was used. Measurements of the b phase (defined in Figure 3.1) were made for the LONGSHOT event as recorded at the stations. The C_S was then computed according to

$$C_S^{(j)} = \frac{b^{(j)}\ \Delta_j}{b^{(HNME)}\ \Delta_{HNME}}$$

The station HNME was chosen for the normalization because it is beyond the triplications for NTS events. We were unable to compute C_S for WHY2K since it is within the triplication range for LONGSHOT. We are attempting to collect more data

TABLE A.1

THE RATIO R_{TZ} (STATION CRITERION #1) OF MAXIMUM VERTICAL AND TANGENTIAL AMPLITUDES

Station	Vertical Z (mu)	Tangential T (mu)	Ratio R_{TZ}
RKON	4617	642	0.14
CPSO	681	75	0.11
WH2YK	224	29	0.13
FNWV	79	36	0.46
HNME	782	---	---

TABLE A.2

VISUAL ESTIMATES OF CODA DURATION, T_C (STATION CRITERION #2)

Station	T_C (sec)
RKON	5
CPSO	> 30
WH2YK	> 30
FNWV	> 30
HNME	5

TABLE A.3

THE STATION CORRECTION C_S AS DETERMINED FROM OBSERVATIONS OF LONGSHOT

Station	Range (km)	b microns	C_S
RKON	5724	0.22	1.00
HNME	7442	0.17	1.00
FNWV	7470	0.055	0.32
WH2YK	2958	0.04	----
CPSO	(Clipped)	----	----

(perhaps explosions in the USSR) to better define C_S for these stations.

On the basis of the tabulated values, it appears that FNWV should be classified as a poor station. More data should be examined in the manner suggested here to clearly evaluate the quality of these sites.

APPENDIX B

MODIFICATION OF SHORT PERIOD BODY WAVES BY CRUSTAL REVERBERATIONS AT THE RECEIVER

It is clear that the amplitude and frequency content of teleseismic body waves are affected to some degree by crustal reverberations in the receiver vicinity. Less clear is the form that this modification can take under circumstances likely to be encountered.

Crustal reverberations can be due to both two-dimensional layering which can be accounted for by plane horizontal layered earth models and three-dimensional structure which cannot. In the following pages are given some examples of the effect of certain variations of a plane layered crustal model. Some insight is then provided into the kinds of effects to be expected from two-dimensional layering at the receiver.

The initial model of the crust at the receiver is given in Table B.1. New models will be formed by modifying this profile.

TABLE B.1

RECEIVER REGION CRUSTAL MODEL A

Depth (km)	Thickness (km)	V_p (km/sec)	V_s (km/sec)	ρ (gm/cm^3)
2.58	2.58	5.0	3.0	2.55
4.84	2.26	5.42	3.27	2.60
11.61	6.77	5.80	3.45	2.60
20.0	8.39	6.0	3.50	2.80

Effects of Sediments at the Surface

For the initial example, consider a PILEDRIVER-like source. That is, the source is characterized by a small P-pP lag. Let the upper mantle effect be included by a constant factor which accounts for geometric spreading and take T/Q = 0.9. The result is a very simple teleseismic short period seismogram. For the calculations the ray parameter p = 0.079 sec/km.

To study the effect of the receiver crust, the crustal model of Table B.1 is modified by replacing the first layer by a sedimentary layer of varying thickness. The thickness of the second layer (V_p = 5.42 km/sec) is adjusted to compensate and the total structure continues to be made up of four layers. For example, when the first layer is 1.29 km thick, the second layer is increased to a thickness of 3.55 km. The sediments have the following properties: V_p = 3.67, V_s = 2.31, ρ = 2.4.

The resulting seismograms are shown in Fig. B.1 and the amplitude data are summarized in Table B.2.

TABLE B.2

THE EFFECT OF A SURFICIAL SEDIMENTARY LAYER ON A SEISMOGRAM TYPICAL OF THE PILEDRIVER EVENT

Thickness (km)	b	T_0 (sec)	c	T_1 (sec)	b/c
0.0	1.00	0.72	1.32	0.81	1.32
0.2	1.21	0.75	1.36	0.78	1.12
0.4	1.23	0.75	1.36	0.78	1.11
0.65	1.18	0.70	1.88	0.81	1.59
1.29	1.44	0.78	1.88	0.92	1.31
2.58	1.34	0.76	1.67	0.82	1.25

The amplitudes of the b (first cycle) and c (second cycle) phases were measured from the seismograms and corrected for instrument response. The latter correction is made by dividing the amplitude by the instrument response at the apparent period, T_0 for b and T_1 for c, measured from the seismograms. Since the absolute amplitudes have little meaning, all values were normalized to the b amplitude of the first case.

In analyzing this example, it is of interest to note that the reflection coefficient for converting the emerging wave into vertical ground motion is nearly the same for the two cases. For the granite cap it is 1.80 and increases only to 1.88 for the sedimentary cap. If the top layer were many wavelengths thick, one expects the displacement change to be proportional to the η ratio ($\eta = V_p^{-2} - p^2)^{1/2}$ which, in this case, is 1.42. For all the cases considered, interference phenomena play an important part.

Effect of a Low Velocity Zone in the Crust

For the second example, we shall take a DIAMOND SCULLS-like source. In this case the P - pP lag is $\simeq$ 0.4 sec, about twice that for PILEDRIVER. A constant geometric spreading factor is again used to account for the upper mantle and, again, T/Q = 0.9. The ray parameter p = 0.079 sec/km, the same as for the previous example.

The basic crustal model to be used is tabulated in Table B.3. It is nearly the same as Model A of Table B.1 which was used for the first example.

TABLE B.3

RECEIVER REGION CRUSTAL MODEL B

Depth (km)	Thickness (km)	V_p (km/sec)	V_s (km/sec)	ρ (gm/cm^3)
2.5	2.5	5.0	2.8	2.5
10.0	7.5	5.4	3.3	2.6
12.0	2.0	5.8	3.45	2.6
20.0	8.0	6.0	3.5	2.8

Model B is then modified by inserting a low velocity layer (V_p = 3.3, V_s = 1.8, ρ = 2.3) of varying thickness at a depth of 2.5 km. The thickness of the next layer (V_p = 5.4) is then varied to keep the interface between V_p = 5.4 and V_p = 5.8 layers at a 10 km depth. This is a rather extreme example, but is useful in delineating the kinds of effects to be expected from low velocity zones in the crust.

The seismograms are shown in Fig.B.2 and the amplitude data are summarized in Table B.4.

TABLE B.4

EFFECT OF A LOW VELOCITY ZONE ON A SEISMOGRAM TYPICAL OF THE DIAMOND SCULLS EVENT

Thickness (km)	b	T_0	c	T_1	b/c
0.0	1.0	0.84	1.98	0.88	1.98
1.0	0.83	0.80	1.75	0.90	2.11
2.5	0.87	0.82	1.80	0.90	2.07
5.0	0.87	0.82	1.78	0.90	2.05
7.5	0.85	0.82	1.77	0.90	2.08
8.5*	0.82	0.82	1.71	0.88	2.09

The low velocity zone has almost no effect on the frequency content of the record. However, the amplitude is reduced by 10-20 percent, seemingly independent of the thickness of the low velocity layer. The travel time is also affected as is apparent from the seismograms, Fig. B.2.

*The low velocity layer extends 1 km into the thick (V_p = 5.8) layer of the crustal model of Table 3.

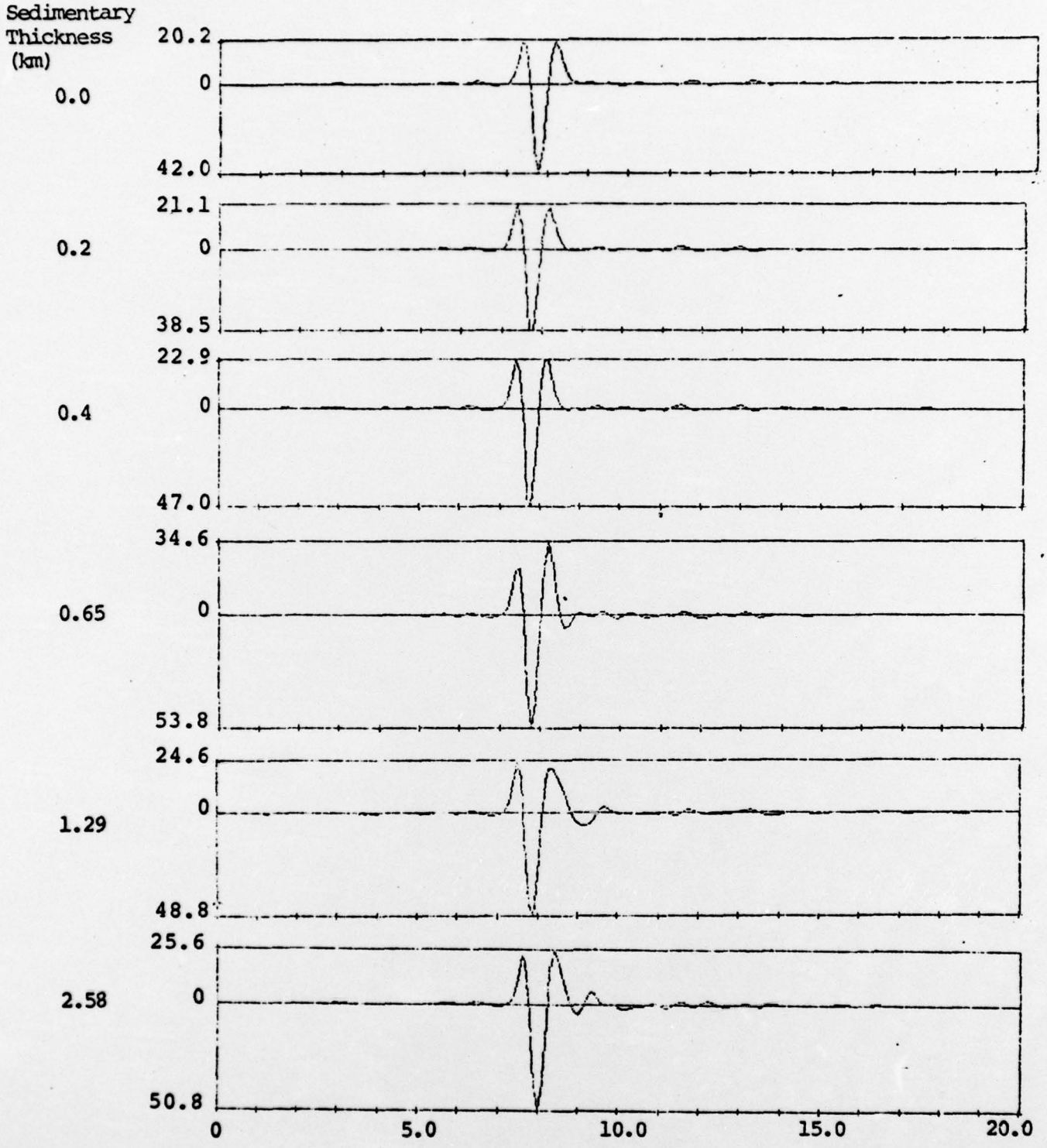

Figure B.1. Synthetic seismograms illustrating the effect of a surficial sedimentary layer at the receiver.

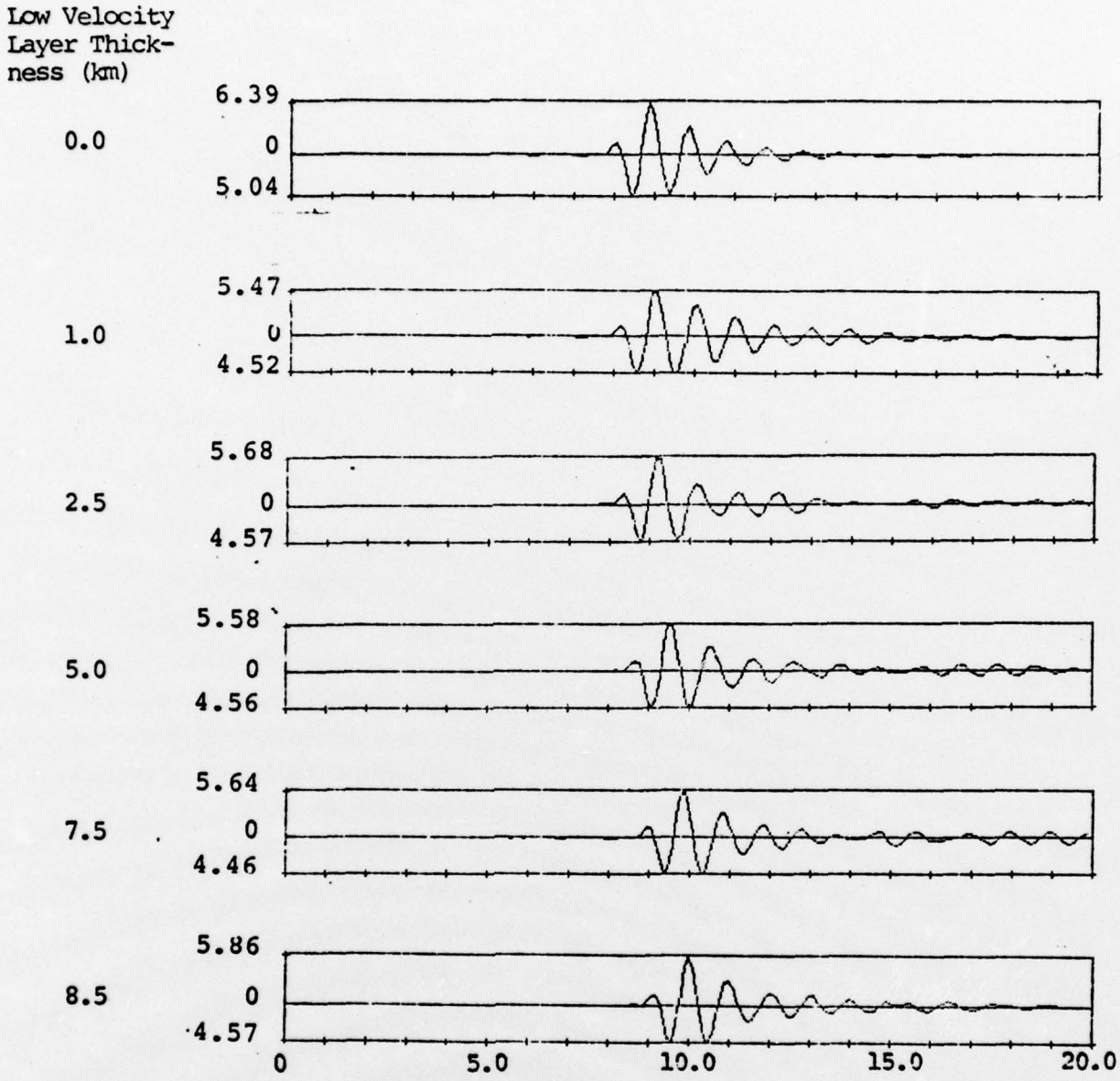

Figure B.2. Synthetic seismograms illustrating the effect of the presence of a low velocity zone in the crust below the receiver. The low velocity zone is of the indicated thickness and begins 2.5 km below the surface.